Tian, Q., Zhang, Y., Chen, L., Flores, P., Dynamics of spatial flexible multibody systems with clearance and lubricated spherical joints. Computers and Structures, Vol. 87(13-14), pp. 913-929, 2009 (DOI: 10.1016/j.compstruc.2009.03.006)

Abstract

A computational methodology for analysis of spatial flexible multibody systems, considering the effects of the clearances and lubrication in the system spherical joints, is presented. The dry contact forces are evaluated through a Hertzian-based contact law, which includes a damping term representing the energy dissipation. The frictional forces are evaluated using a modified Coulomb's friction law. In the case of lubricated joints, the resulting lubricant forces are derived from the corresponding Reynolds' equation. An absolute nodal formulation is utilized in flexible body formulation. The generalized-**α** method is used to solve the resulting equations of motion. The effectiveness of the methodology is demonstrated by two numerical examples.

Keywords: Clearance; Spherical joints; Lubricated joints; Reynolds' equation; Generalized-**α** method; Absolute nodal coordinate formulation

1. Introduction

Ideal kinematic joints in any mechanical system allow relative motion between the components. Due to the manufacturing tolerances, wear or material deformations these joints are not perfect and inherently have some clearances. These clearances affect the dynamic response of the system and eventually lead to important deviations between the projected behavior of the mechanisms and their real outcome [1-4]. The contact-impact phenomenon associated with clearances directly affects the service life of a mechanism, since it is usually the cause of vibrations, noise and wear, resulting in an increase of maintenance costs [5-7]. The attenuation of the impact response and of the vibration characteristics in industrial machines is obtained by including treatment of joint clearances in their design. The presence and treatment of clearance in joints is a complex and important problem in the realistic modeling of multibody systems. This is a key issue due to the demand for the proper design of the real joints in many industrial applications [8-10].

The serious consequences of the joint clearances on the dynamic behavior of the mechanical systems, along with the subject of the clearance physical representation, have stimulated and attracted the attention of a large number of researchers over the last few years. Indeed, a number of theoretical and experimental works devoted to the dynamics research of multibody mechanical systems with realistic joints has been published recently [10]. Some of them focus upon the systems in which only one joint is modeled as a realistic joint. Liu et al. [11] developed a simple contact force formulation of the spherical clearance joints in multibody mechanical systems, using the distributed elastic forces to model the compliant of the surfaces in contact. Flores et al. [12] also presented a methodology to assess the influence of the spherical joint clearances in spatial multibody systems. Both of these approaches are only valid for the case of dry contact between the socket and ball. Flores et al. [13] extended their work to include a general methodology for modeling lubricated revolute joints in constrained rigid multibody systems. Based on neural network and genetic algorithms, Erkaya Uzmay [14, 15] investigated the influence of joint clearances on the mechanism path generation and transmission angle. In this case, the joint clearances

are modeled as a massless virtual link. The thermal effect of high temperature on mechanisms having joint clearances was studied by Bing and Ye [16]. They demonstrated that by increasing the combined clearance of the revolute joint, a favorable reduction of the friction torque between the bush and shaft can be obtained for normal operation conditions of a reheat-stop-valve mechanism. However, if the temperature of steam reaches to 650°C, the friction torque between the bush and the shaft becomes larger and the sticking phenomenon exists. In [17], a methodology, based on the Archard's model, was presented for studying and quantifying the wear phenomenon in revolute joint clearances. The results of this study indicate that the wear phenomenon is not uniformly distributed around the joint surface, owing to the fact that the contact between the joint elements is wider and more frequent in some specific regions.

One of the most important issues for the dynamics research on the multibody systems with joint clearances is how to model the contact-impact phenomenon. Many researchers have proposed different kinds of models such as Kelvin-Voigt model [5, 6], the three modes model [18], the model based on the restitution coefficient and momentum method [19], but they all have their own disadvantages. For example, for the Kelvin-Voigt model it is difficult to quantify the parameters of the spring and damper elements and it inherently does not represent the nonlinear nature of the contact-impact process. While the model based on the restitution coefficient and momentum-based method assumes that no change in the realistic configuration between contacting bodies occurs during the period of contact-impact, which is not true for joint clearances. Lankarani and Nikravesh [20] developed a continuous contact force model with hysteresis damping for impact in multibody systems. The model uses the general trend of the Hertz contact law, in which a hysteresis damping function is incorporated with the intent to represent the energy dissipated during the impact. Based on this continuous contact model, Flores and Ambrósio [1] studied the dynamic characteristics of multibody systems with joint clearances. More recently, this continuous contact-impact model has also been successfully used to carry out the wheel-rail contact-impact dynamics research [21].

It is important to note that all the above mentioned studies have been done based on the rigid body dynamics principle. The deformations associated with the flexibility of the bodies need to be studied while may lead to different dynamics characteristics, especially as far as the large deformations are concerned. Thus, some studies have included the influence of the flexibility of the bodies in the dynamic performance of multibody systems containing gaps in the joints. Dubowsky and Gardner [22] developed a dynamic model for an elastic linkage mechanism with clearance connections by Lagrangian approach. This model is quite comprehensive and complicated and needs to be simplified for possible numerical implementation. Dubowsky et al. [23] applied the perturbation method, treating the angular motion caused by clearances and elastic deformations as small quantities and neglecting the high order and high-frequency responses of the small variables. This method simplifies the dynamics equations, but is not suitable for the conditions of large elastic deformations or large clearances. Dubowsky and Moening [24] obtained a reduction in the impact force level by introducing flexibility of the bodies. They also observed a significant reduction of the acoustical noise produced by the impacts when the system incorporates flexible bodies. Kakizaki et al. [25] presented a model for spatial dynamics of robotic manipulators with flexible links and joint clearances, where the effect of the clearance is taken into account in controling the robotic system. Bauchau and his co-workers [26, 27] also established a systematic approach considering the flexibility of the bodies based on the finite element method and lubrication conditions. Liu and Lin [28] studied the dynamic performance of planar flexible mechanisms with revolute joint clearances based on the finite element method. The lubrication effect in joints was also considered in this study. Shiau et al. [29] presented a dynamic analysis of a 3-PRS series-parallel mechanism including flexibility of the bodies, clearances and friction. They demonstrated that the dynamic response of the system degrades as the joint clearances increase, and the joint contact forces increase with the joint clearances and friction coefficient. Thus, proper modeling of joint clearances in multibody systems is required to achieve better understanding of the dynamic performance of the machines and mechanisms.

Almost all of the aforementioned studies, on the dynamics performance of the flexible multibody system with joint clearances are based on the traditional finite element theory, in which the system is assumed to undergo small deformations and rotations. It has been demonstrated that the traditional finite element method can not describe the behavior of flexible multibody system with large deformation and rotation configuration with accuracy [30]. Shabana [31, 32] proposed a simple procedure, the absolute nodal coordinate formulation (ANCF), that employs the definition of the slopes to define the element coordinates instead of the infinitesimal and finite rotations. As the locations and deformations of the material points on the finite element are defined in the global coordinate system, using the element shape functions and the nodal coordinates, the mass matrix within the system equations remains constant and the centrifugal and Coriolis forces vanish [33]. Using the absolute nodal coordinate formulation, the beam, plate, and shell elements can be treated as isoparametric elements and used to describe the exact modeling of the body dynamics. In addition, the description of the joint constraints and forces becomes much simpler based on the ANCF. The ANCF has been considered a benchmark in flexible multibody dynamics development [34, 35], and has been used by several other authors in different contexts [36-38].

In this paper, dynamic modeling and analysis of flexible spatial multibody systems with clearance and lubricated spherical joints is investigated. The absolute nodal coordinated-based spatial beam element is used to derive the equations of motion for the flexible multibody systems with spherical joint clearances. A continuous contact-impact model is used to evaluate the intra-joint contact-impact forces, in which the energy dissipation in the form of a hysteresis damping is considered. The frictional effect is included based on a modified Coulomb's friction law. The lubrication effect in the spherical joint clearance is included by using the Reynolds' equation. To dissipate the spurious high-frequency responses and to preserve the low-frequency responses, the generalized-$\boldsymbol{\alpha}$ method is utilized in the simulations. The paper is organized as follows. In section 2 the spatial ANCF-based beam element is briefly revisited. Full description of the spatial joints with clearance

for the dry contact situation is presented in section 3. A model for the treatment of lubricated spherical joints is provided in section 4. Section 5 deals with the computational strategy for the assembly and solution of the equations of motion for the corresponding constrained flexible spatial multibody systems. Section 6 presents two numerical examples, namely a spatial double pendulum and a spatial four-bar mechanism, which incorporate ideal, clearance, and lubricated joints. To verify the validity of the model for the stiff systems, the results based on the absolute nodal coordinated-based model are compared with the results obtained by using the MSC.ADAMS software. Finally, in the last section the main conclusions from this study are drawn, in the light of the assumptions and procedures underpinning this research, and the perspectives for future research are then outlined.

2. Spatial ANCF-based beam element

The main purpose of this section is to look at the most fundamental aspects of the spatial ANCF-based beam element. The absolute nodal coordinate formulation has been developed for modeling dynamic systems of large-displacement and large-rotation problems in flexible multibody systems, because the conventional finite element method deals with the small-displacement problems. The first spatial beam type finite element developed in the context of the ANCF [39, 40] was parameterized as a volume. It has been shown that this element suffers from some numerical problems such as shear or Poisson locking effects and, nowadays, there are several implementations of this element that have enabled prevention of these problems [41, 42]. However, the numerical problems associated with this element can be avoided or, at least, reduced by increasing the number of elements used to discrete the flexible part. In this work, the original element developed by Shabana and Yakoub [39] is used as the kinematic description. It is the same as that of others, its formulation is simpler, and only differs from the new elements in the formulation of the elastic forces. Furthermore, it is quite easy to extend this method to other type spatial beam elements. Figure 1 illustrates the ANCF-based spatial beam element.

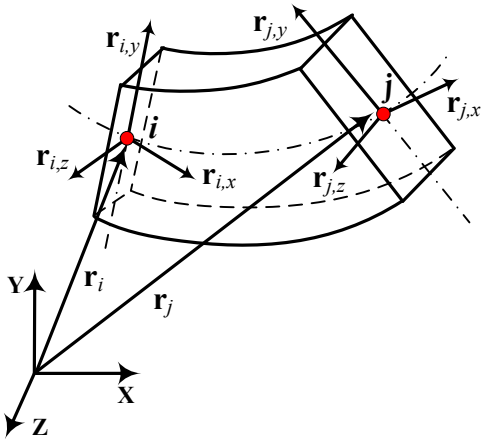

Fig. 1. Spatial ANCF-based beam element.

As it is observed in Fig. 1, there are two nodes *i* and *j* in the element. The nodal coordinates vector **e** includes the node position vector $\mathbf{r}_i$ and $\mathbf{r}_j$, as well as the partial derivatives of the position vector ($\mathbf{r}_{i,x}$, $\mathbf{r}_{i,y}$, $\mathbf{r}_{i,z}$, $\mathbf{r}_{j,x}$, $\mathbf{r}_{j,y}$ and $\mathbf{r}_{j,z}$) with respect to the three local coordinates or parameters of the element. Then the coordinate vector **e** can be expressed as,

$$\mathbf{e} = [\mathbf{e}_i \ \ \mathbf{e}_j]^T = [\mathbf{r}_i, \mathbf{r}_{i,x}, \mathbf{r}_{i,y}, \mathbf{r}_{i,z}, \mathbf{r}_j, \mathbf{r}_{j,x}, \mathbf{r}_{j,y}, \mathbf{r}_{j,z}]^T \tag{1}$$

Since for each node there are 12 nodal coordinates, then the coordinate vector **e** can also be expressed as,

$$\begin{aligned}\mathbf{e} = [&r_{i1}, r_{i2}, r_{i3}, \frac{\partial r_{i1}}{\partial x}, \frac{\partial r_{i2}}{\partial x}, \frac{\partial r_{i3}}{\partial x}, \frac{\partial r_{i1}}{\partial y}, \frac{\partial r_{i2}}{\partial y}, \frac{\partial r_{i3}}{\partial y}, \frac{\partial r_{i1}}{\partial z}, \frac{\partial r_{i2}}{\partial z}, \frac{\partial r_{i3}}{\partial z}, r_{j1}, r_{j2}, r_{j3}, \\ &\frac{\partial r_{j1}}{\partial x}, \frac{\partial r_{j2}}{\partial x}, \frac{\partial r_{j3}}{\partial x}, \frac{\partial r_{j1}}{\partial y}, \frac{\partial r_{j2}}{\partial y}, \frac{\partial r_{j3}}{\partial y}, \frac{\partial r_{j1}}{\partial z}, \frac{\partial r_{j2}}{\partial z}, \frac{\partial r_{j3}}{\partial z}]^T.\end{aligned} \tag{2}$$

The position vector in the global coordinate framework *XYZ* of an arbitrary point of the element is given by,

$$\mathbf{r} = \mathbf{S}\mathbf{e} \tag{3}$$

in which **S** is the element shape function. Finally, by using Newton-Euler formulation, the element equations of motion can be written as,

$$\mathbf{M}_e \ddot{\mathbf{e}} = \mathbf{Q}_e - \mathbf{F}_e \tag{4}$$

where $\mathbf{M}_e = \int_v \rho \mathbf{S}^T \mathbf{S} dv$ compensates the element constant mass matrix (ρ is mass

density and v denotes the volume), $\mathbf{F}_e$ is the element elastic force vector which can be deducted by continuum mechanics approach [43], and $\mathbf{Q}_e$ represents the element external generalized force vector. The interested reader in the details of the ANCF is referred to the works by Shabana [30-33, 39, 40].

3. Spherical joints with clearance: dry contact model

In order to consider the contact-impact forces into the equations of motion for flexible multibody systems based on the ANCF, it is first necessary to develop a mathematical model for joints with clearance. Thus, let consider Fig. 2 in which the socket and the ball elements of a spherical joint clearance are shown.

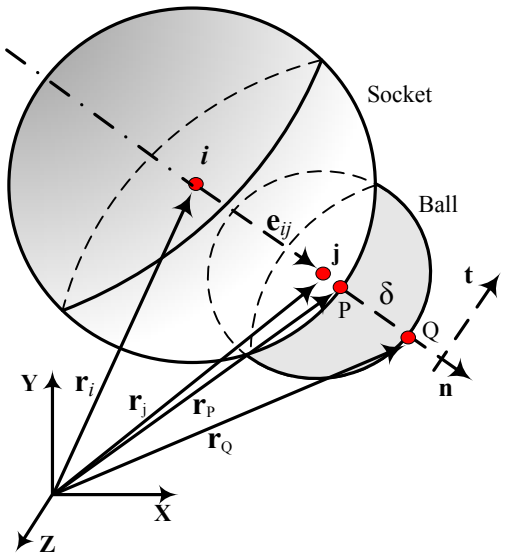

Fig. 2. The socket and the ball of a spherical joint clearance in the ANCF-based framework.

Based on the ANCF formulation, node i indicates the center of the socket, and the center of the ball is located at node j. The vectors **n** and **t** represent the normal and tangential directions to the contacting surfaces, respectively. From Fig. 2, the eccentricity vector, $\mathbf{e}_{ij}$, which connects the centers of the socket and the ball, can be calculated as,

$$\mathbf{e}_{ij} = \mathbf{r}_\mathrm{j} - \mathbf{r}_\mathrm{i} = [e_x \quad e_y \quad e_z]^T \tag{5}$$

Thus, the magnitude of the eccentricity vector is given by,

$$e_{ij} = \sqrt{\mathbf{e}_{ij}^T \mathbf{e}_{ij}} = \sqrt{e_x^2 + e_y^2 + e_z^2} \tag{6}$$

The unit eccentricity vector **n** is aligned with the eccentricity vector, and, therefore, it can be written as,

$$\mathbf{n} = \frac{\mathbf{e}_{ij}}{e_{ij}} \tag{7}$$

With reference to Fig. 2, the penetration depth due to the contact between the ball and the socket surfaces can be evaluated as,

$$\delta = e_{ij} - c \tag{8}$$

where c is the radial clearance given by $c=R_s-R_b$, in which R_s and R_b are the radius of the socket and the radius of the ball. In Fig. 2, points P and Q indicate the contact points on socket and ball surfaces, respectively. Then, the position of these contact points can be expressed as,

$$\mathbf{r}_{\mathrm{P}} = \mathbf{r}_i + \mathbf{n}R_s \tag{9}$$

$$\mathbf{r}_{\mathrm{Q}} = \mathbf{r}_j + \mathbf{n}R_b \tag{10}$$

Since the contact between the socket and ball is an oblique eccentric collision, its contact-impact treatment involves both relative normal velocity and relative tangential velocity. The velocity of the contact points P and Q, expressed in terms of the global coordinate system, can be obtained simply by differentiating Eqs. (9) and (10) with respect to time, yielding,

$$\dot{\mathbf{r}}_{\mathrm{P}} = \dot{\mathbf{r}}_i + \dot{\mathbf{n}}R_s \tag{11}$$

$$\dot{\mathbf{r}}_{\mathrm{Q}} = \dot{\mathbf{r}}_j + \dot{\mathbf{n}}R_b \tag{12}$$

Then, the relative normal velocity can be expressed as,

$$\mathbf{v}_n = \left[(\dot{\mathbf{r}}_P - \dot{\mathbf{r}}_Q)^T \mathbf{n} \right] \mathbf{n} \tag{13}$$

Similarly, the relative tangential velocity is given by,

$$\mathbf{v}_t = (\dot{\mathbf{r}}_P - \dot{\mathbf{r}}_Q) - \mathbf{v}_n \tag{14}$$

Dividing the eccentricity e_{ij} by radial clearance c yields the eccentricity ratio ε expressed by,

$$\varepsilon = \frac{e_{ij}}{c} \tag{15}$$

By differentiating Eq. (6) with respect to time, and dividing the result by radial clearance, the time rate of change of the eccentricity ratio is expressed as,

$$\dot{\varepsilon} = \frac{\dot{e}_{ij}}{c} \tag{16}$$

It is known that modeling contact forces during an impact event plays a key role in the dynamic analysis of mechanical systems [44]. On the one hand, the contact force model must be computed by using a suitable constitutive law that takes into account material properties of the colliding bodies, geometric characteristics of the impacting surfaces and the impact velocity. On the other hand, the numerical method for the calculation of the contact forces should be stable in order to allow for the integration of the mechanical systems' equations of motion. Various types of constitutive laws are suggested in the literature, being one of the more prominent proposed by Hertz [45]. However, this law is purely elastic in nature and can not explain the energy loss during the impact process. Lankarani and Nikravesh [20] overcame this difficulty by separating the normal contact force into elastic and dissipative components. Thus, in the present study, when impact between the socket and ball occurs, the normal contact forces are evaluated by using the continuous contact model proposed by Lankarani and Nikravesh [20], which can be written as,

$$F_n = K\delta^n \left[1 + \frac{3(1-c_e^2)}{4} \frac{\dot{\delta}}{\dot{\delta}^{(-)}} \right] \tag{17}$$

where c_e is the restitution coefficient, $\dot{\delta}^{(-)}$ represents the initial impact velocity, $\dot{\delta}$ denotes the relative penetration velocity, n is a specified nonlinear index, and the stiffness coefficient K for two spherical contacting bodies can be expressed by,

$$K = \frac{4}{3(\eta_b + \eta_s)} \left[\frac{R_b R_s}{R_b + R_s} \right]^{1/2} \tag{18}$$

in which η_b and η_s are the material parameters for ball and socket, respectively, and can be given by,

$$\eta_k = \frac{1-\nu_k^2}{E_k}, \qquad (k=b,s) \tag{19}$$

ν_k and E_k represent the Poisson's ratio and the material Young's modulus associated with the ball and the socket. Then, the resulting contact forces are included in the equations of motion of the system as external generalized forces [46].

It should be highlighted that the contact force model considered here that accounts for the energy dissipation is found to be satisfactory for general mechanical contacts. Shivaswamy [47] demonstrated experimentally that at low impact velocities, the energy dissipation due to the internal damping is the main contributor to energy loss. Moreover, the contact force model given by Eq. (17) is only valid for low impact velocities, that is, speeds that are at the most one order of magnitude lower than the elastic wave traveling velocity [48, 49]. Recently, Flores et al. [50] carried out a numerical and experimental investigation of multibody systems with joint clearances. They used the same contact-impact force laws as in the present study, being the correlation between the numerical and experimental results quite good. Nevertheless, other contact models are candidates to be used for the normal contact force and some more insight can be obtained from works that have been developed independently of that utilized here. In particular the interested reader can find in the works of Liu et al. [11], Kuwabara and Kono [51] and Ramirez et al. [52] good insights on the collision of spheres where the dissipative effects play an important role.

It is known that frictional forces act when contacting bodies tend to slide relative each other. These forces are tangential to the surfaces of contact and are opposite to the sliding velocity. The tangential forces due to the friction phenomenon may be considered when the impact velocity has a relative tangential component, such as in the case of oblique eccentric collisions. Friction is a quite complex phenomenon which involves interaction between the surfaces of contacting bodies and may lead to different friction regimes such as sliding and stiction [53]. The most fundamental and simplest frictional force model is the Coulomb's friction law [54]. This model

assumes that the frictional force between sliding bodies with respect to each other is proportional to the normal contact force. The constant of proportionality is called the friction coefficient. However, the definition of the Coulomb's friction law poses numerical difficulties when the relative tangential velocity is in the vicinity of zero. Thus, in the present work in order to avoid numerical difficulties, the friction effect is included as a modified Coulomb's friction law [55] as,

$$\mathbf{F}_t = -c_f c_d F_n \frac{\mathbf{v_t}}{\|\mathbf{v_t}\|} \tag{20}$$

where c_f is the friction coefficient, and dynamic correction coefficient c_d is given by,

$$c_d = \begin{cases} 0 & \text{if } \|\mathbf{v}_t\| \le v_0 \\ \dfrac{\|\mathbf{v}_t\| - v_0}{v_1 - v_0} & \text{if } v_0 \le \|\mathbf{v}_t\| \le v_1 \\ 1 & \text{if } \|\mathbf{v}_t\| \ge v_1 \end{cases} \tag{21}$$

in which, v_0 and v_1 are given tolerances for the relative tangential velocity of the surfaces in contact. This dynamic correction factor effectively prevents that the frictional force changes direction for almost null values of the tangential velocity. Therefore, the great merit of the modified Coulomb's law expressed by Eq. (20) is that it allows the numerical stabilization of the integration algorithm. This frictional force model does not account for other tribological phenomena like the adherence between the sliding contact surfaces.

Figure 3 shows the frictional force and its components acting on the socket and the ball. The spatial friction force can be expressed in its Cartesian coordinates as,

$$\mathbf{F}_t = [F_{tx} \quad F_{ty} \quad F_{tz}]^T \tag{22}$$

Form Fig. 3, the position vector $\mathbf{R}_n$ can be written as,

$$\mathbf{R}_n = [R_x \quad R_y \quad R_z]^T \tag{23}$$

The direction of this vector can be determined by using the unit eccentricity vector **n** described earlier. Thus, if the frictional force is acting at a point *P*, it is necessary to transform it into the force acting at node *k*, taking into account the corresponding

moments that are generated in the process. With regard to Fig. 3, the three moments generated by the friction force and that are applied to the node *k* can be written as,

$$M_X = F_{ty}R_z - F_{tz}R_y \tag{24}$$

$$M_Y = F_{tz}R_x - F_{tx}R_z \tag{25}$$

$$M_Z = F_{tx}R_y - F_{ty}R_x \tag{26}$$

Finally, based on the formulation presented in [54], these frictional moments can be easily transformed into the generalized forces.

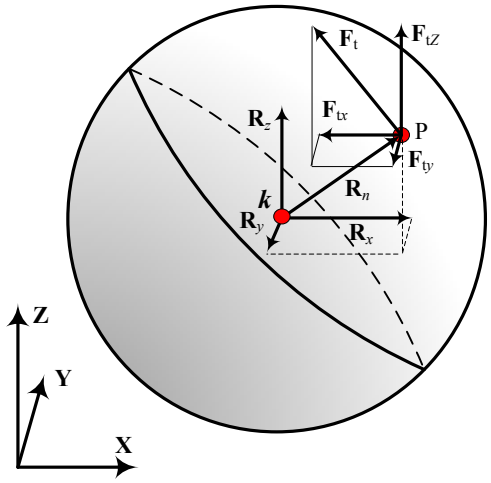

Fig. 3. Representation of the frictional force components.

4. Spherical joints with clearance: lubricated model

Generally, in order to avoid or at least minimize the ball-socket direct contact and extend spherical joint lifetime, lubricants are often used for any practical application. Therefore, proper modeling of lubricated spherical joints in multibody systems is necessary to achieve a better understanding of their dynamic performance. In this section, a mathematical model for spherical joints with clearance, taking into account the lubrication action, is presented. Figure 4 shows a spherical joint in which the space between the ball and socket wall is filled with a lubricant. The socket and ball centers are denoted by *i* and *j*, respectively. Furthermore, a spherical coordinate system is adopted to model the lubrication force components, as it can be observed in

Fig. 4. Thus, the position of an arbitrary point *P* located inside the joint boundaries can be determined by its spherical coordinates (r, θ, ϕ). Since lubrication force has to be evaluated by integrating the Reynolds' equation and because the fluid lubricants can not support negative pressure, the pressure field is integrated only over the positive part by setting the pressure in the remaining portion equal to zero. This corresponds to Gümbel's boundary conditions [57, 58]. In fact, complete or full film does not take into account the cavitation phenomenon and, consequently, contemplate the existence of negative pressures, but this case is not realized in many applications due to the fluid incapacity to sustain significant sub-ambient pressures [10].

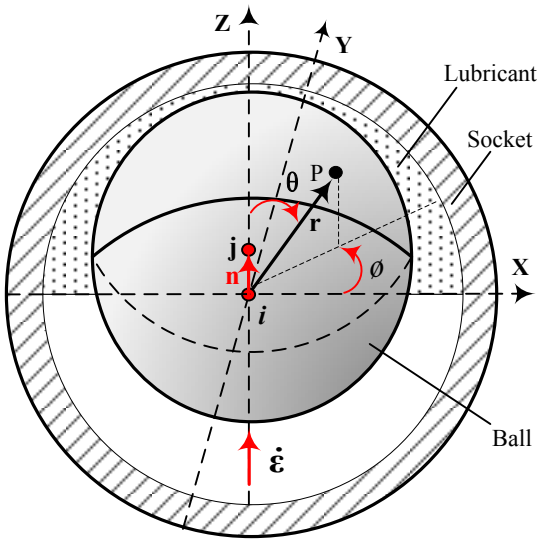

Fig. 4. Schematic representation of a lubricated spherical joint.

For the case of lubricated spherical joints, the full general form of the isothermal Reynolds' equation can be stated as [57, 58],

$$\frac{1}{R_s^2}\left[\frac{1}{\sin\theta}\frac{\partial}{\theta}\left(\frac{h^3}{12\mu}\sin\theta\frac{\partial p}{\partial\theta}\right)+\frac{1}{\sin^2\theta}\frac{\partial}{\phi}\left(\frac{h^3}{12\mu}\frac{\partial p}{\partial\phi}\right)\right]= \\ =\frac{1}{R_s\sin\theta}\left(h\cos\theta\bar{U}^{\theta}+h\sin\theta\frac{\partial\bar{U}^{\theta}}{\partial\theta}+h\frac{\partial\bar{U}^{\phi}}{\partial\phi}+\sin\theta\bar{U}^{\theta}\frac{\partial h}{\partial\theta}+\bar{U}^{\phi}\frac{\partial h}{\partial\phi}\right)+\frac{\partial h}{\partial t} \tag{27}$$

from which it is possible to obtain the following expressions,

$$2\bar{U}^{\theta}=-R_s\omega^x\sin\phi+R_s\omega^y\cos\phi \tag{28}$$

$$2\bar{U}^{\phi} = -R_s\omega^x \cos\phi\cos\theta - R_s\omega^y \sin\phi\cos\theta + R_s\omega^z \sin\theta \tag{29}$$

$$h = c(1-\varepsilon^x \sin\theta\cos\phi - \varepsilon^y \sin\theta\sin\phi - \varepsilon^z \cos\theta) \tag{30}$$

where p denotes the lubricant pressure, r, θ and ϕ are the spherical coordinates h is the lubricant thickness, μ is the dynamic lubricant viscosity, ε^x, ε^y and ε^z are the components of the eccentricity vector in the X, Y and Z directions, and ω^x, ω^y and ω^z represent the angular velocity components in the X, Y and Z directions.

Based on Eq. (15), the ε^x, ε^y and ε^z components can be evaluated by,

$$\boldsymbol{\varepsilon} = \varepsilon\mathbf{n} = [\varepsilon^x, \varepsilon^y, \varepsilon^z]^T \tag{31}$$

As mention above, the boundary condition for the hemispherical socket lubricant pressure are defined by [58],

$$p\left(r, \frac{\pi}{2}, \phi\right) = 0 \tag{32}$$

Under the assumption of the pure squeeze condition, the lubrication force generated by the rotation motion can be neglected, and, consequently, the pressure field can be expressed as,

$$p = \begin{cases} \dfrac{3\mu\dot{\varepsilon}R_s^2}{c^2\varepsilon}\left[\dfrac{1}{(1-\varepsilon\cos\theta)^2} - 1\right] & if\ \varepsilon \neq 0 \\ \dfrac{6\mu\dot{\varepsilon}R_s^2}{c^2}\cos\theta & if\ \varepsilon = 0 \end{cases} \tag{33}$$

Finally, the squeeze lubrication force can be obtained by integrating the pressure,

$$\begin{aligned} F_{squeeze} &= R_s^2 \int_0^{2\pi}\int_0^{\frac{\pi}{2}} p\cos\theta\sin\theta d\theta d\phi \\ &= \begin{cases} \dfrac{6\pi\mu R_s^4\dot{\varepsilon}}{c^2}\left[\dfrac{1}{\varepsilon^3}\ln(1-\varepsilon) + \dfrac{1}{\varepsilon^2(1-\varepsilon)} - \dfrac{1}{2\varepsilon}\right] & if\ \varepsilon \neq 0 \\ \dfrac{4\pi\mu R_s^4\dot{\varepsilon}}{c^2} & if\ \varepsilon = 0 \end{cases} \end{aligned} \tag{34}$$

where μ is the dynamic lubricant viscosity, being the remaining parameters associated with the joint kinematics. As it can be seen in Fig. 4, when $\dot{\varepsilon}$ is in the same direction as the unit eccentricity vector $\mathbf{n}$, the lubrication force can be calculated according to

Eq. (34), while when $\dot{e}_{ij}$ is in the opposite direction of the unit eccentricity vector **n**, the squeeze lubrication force is set to zero.

As the fluid film thickness can become very thin, that is, the ball is very close to the socket surface, the squeeze force due to the lubricant evaluated from Eq. (34) becomes very large (since ε is very close to 1). Consequently, the squeeze force will approach infinity, ultimately leading to simulation divergence. In order to solve this problem, a model that smoothes the transition between the lubricated and dry contact cases is considered, which is schematically represented in Fig. 5. This model, which combines the squeeze-film action and the dry contact effect, was first proposed in [59]. It should be noted that this approach ensures continuity in the joint reaction force when the squeeze force model is switched to dry contact force model.

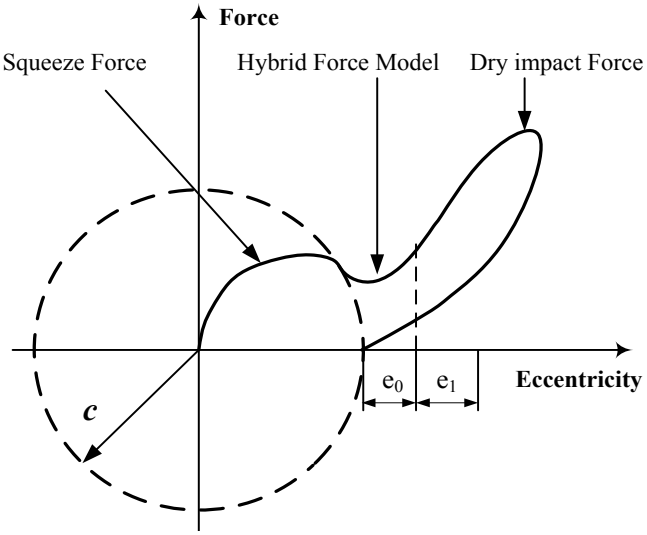

Fig. 5. Transition model between lubricated and dry contact models.

Mathematically, the transition force model can be written as,

$$F = \begin{cases} F_{squeeze} & if\ e_{ij} \le c \\ \dfrac{(c+e_0)-e_{ij}}{e_0} F_{squeeze} + \dfrac{e_{ij}-c}{e_0} F_{dry} & if\ c \le e_{ij} \le c+e_0 \\ F_{dry} & if\ e_{ij} \ge c+e_0 \end{cases} \tag{35}$$

where e_0 and e_1 are given eccentricity tolerances. The values of these parameters must be chosen carefully, since they depend strongly on the clearance size. It should be noted that the clearance used for the squeeze-film model is not c, but it is c+e_1 instead.

5. Computational strategy to solve the equations of motion

This section deals with the computational strategy for the numerical solutions of the equations of motion of spatial flexible multibody systems including spherical joints with clearance and lubrication. As it has already been mentioned, based on the ANCF, the assembly of the elements can be carried out by traditional finite element method. The element nodal coordinates **e** can be easily transformed into the flexible multibody system generalized coordinates **q**. Thus, based on the previous works on ANCF, the equations of motions for constrained flexible multibody systems can be expressed in a compact form as [33, 43],

$$\begin{cases} \mathbf{M}\ddot{\mathbf{q}} + \boldsymbol{\Phi}_{\mathbf{q}}^{T}\boldsymbol{\lambda} + \mathbf{F}(\mathbf{q}) = \mathbf{Q}(\mathbf{q}) \\ \boldsymbol{\Phi}(\mathbf{q}, t) = \mathbf{0} \end{cases} \tag{36}$$

where $\mathbf{M}$ is the system mass matrix, $\boldsymbol{\Phi}(\mathbf{q},t)$ is the vector that contains the system constraint equations corresponding to ideal or perfect joints, $\boldsymbol{\Phi}_{\mathbf{q}}$ is the derivative matrix of constraint equations with respect to the system generalized coordinates $\mathbf{q}$, vector $\boldsymbol{\lambda}$ is Lagrangian multipliers associated with the constraints, and $\mathbf{Q}(\mathbf{q})$ denotes the system external generalized forces. In the present study, vector $\mathbf{Q}(\mathbf{q})$ includes the distributed gravitational force as well as the contact-impact force, and $\mathbf{F}(\mathbf{q})$ contains the system elastic force vector.

It should be highlighted that the process of solving the equations of motion in the case of flexible bodies differs from the case in which the bodies are considered as rigid and with joint clearances. This is due to the fact that in the above equations of motion for flexible multibody systems with joint clearances, the spurious high-frequency responses are stimulated, which is mainly caused by the continuous high-frequency contact-impact forces. In addition, the spurious high-frequency response is also a product of the finite element discretization. The convergence for the solution of the high-frequency modes is poor if the spurious high-frequency responses could not be damped out. As a consequence, the high-frequency responses produce artificially extreme large impact forces, which in turn lead to the divergence of the simulation. Therefore, it is desirable for an algorithm to have a controllable numerical

dissipation in the high-frequency range, that is, the low-frequency responses should be well-preserved and the high-frequency responses should be damped in a controllable way. Thus, according to the generalized-$\boldsymbol{\alpha}$ method, it is possible to write [60],

$$(1-\alpha_m)\mathbf{a}_{n+1}+\alpha_m\mathbf{a}_n=(1-\alpha_f)\ddot{\mathbf{q}}_{n+1}+\alpha_f\ddot{\mathbf{q}}_n \text{ , } \mathbf{a}_0=\ddot{\mathbf{q}}_0 \tag{37}$$

$$\mathbf{q}_{n+1}=\mathbf{q}_n+h\dot{\mathbf{q}}_n+h^2((\frac{1}{2}-\beta)\mathbf{a}_n+\beta\mathbf{a}_{n+1}) \tag{38}$$

$$\dot{\mathbf{q}}_{n+1}=\dot{\mathbf{q}}_n+h((1-\gamma)\mathbf{a}_n+\gamma\mathbf{a}_{n+1}) \tag{39}$$

where n denotes the *nth* iteration, β, γ, α_f and α_m are the algorithm parameters. In order to make the generalized-$\boldsymbol{\alpha}$ algorithm second-order accurate, to dissipate the spurious high- frequency responses and to well-preserve the low-frequency responses, the parameters in the algorithm can be determined by the following relations,

$$\beta=\frac{(1+\alpha_f-\alpha_m)^2}{4} \tag{40}$$

$$\gamma=\frac{1}{2}+\alpha_f-\alpha_m \tag{41}$$

$$\alpha_f=\frac{\sigma}{\sigma+1} \tag{42}$$

$$\alpha_m=\frac{2\sigma-1}{\sigma+1} \tag{43}$$

in which $\sigma\in[0\ \ 1]$, σ=1 will lead to an energy-preserving algorithm and σ=0, the maximum energy will be dissipated by the algorithm [60]. Arnold and Brüls [61] proposed a computational scheme based on the generalized-$\boldsymbol{\alpha}$ method for constrained mechanical systems. In the present study, and based on Arnold and Brüls' work, the Broyden-Newton [62] approach is introduced to the iteration process. The corresponding entire computational scheme is illustrated in the flowchart of Fig. 6. In the process the following relations are utilized,

$$\hat{\beta}=\frac{(1-\alpha_m)}{h^2\beta(1-\alpha_f)} \tag{44}$$

$$\hat{\gamma}=\frac{\gamma}{h\beta} \tag{45}$$

which can make

$$\frac{\partial \ddot{\mathbf{q}}}{\partial \mathbf{q}} = \mathbf{I}\hat{\beta},\ \frac{\partial \dot{\mathbf{q}}}{\partial \mathbf{q}} = \mathbf{I}\hat{\gamma} \tag{46}$$

satisfied. Here, the variable *tol* is the integration error tolerance, **J** is the system Jacobian matrix, and **G** is given by,

$$\mathbf{G} = \begin{bmatrix} \mathbf{M}\ddot{\mathbf{q}} + \boldsymbol{\Phi}_{\mathbf{q}}^{T}\boldsymbol{\lambda} + \mathbf{F}(\mathbf{q}) - \mathbf{Q}(\mathbf{q}) \\ \boldsymbol{\Phi}(\mathbf{q}, t) \end{bmatrix} \tag{47}$$

The Jacobian matrix, after some fundamental mathematical operations, can be written as,

$$\mathbf{J} = \frac{\partial \mathbf{G}}{\partial [\mathbf{q}\ \boldsymbol{\lambda}]^{T}} = \begin{bmatrix} \mathbf{M}\hat{\beta} + \left(\boldsymbol{\Phi}_{\mathbf{q}}^{T}\boldsymbol{\lambda}\right)_{\mathbf{q}} + \left(\mathbf{F}(\mathbf{q}) - \mathbf{Q}(\mathbf{q})\right)_{\mathbf{q}} & \boldsymbol{\Phi}_{\mathbf{q}}^{T} \\ \boldsymbol{\Phi}_{\mathbf{q}} & \mathbf{0} \end{bmatrix} \tag{48}$$

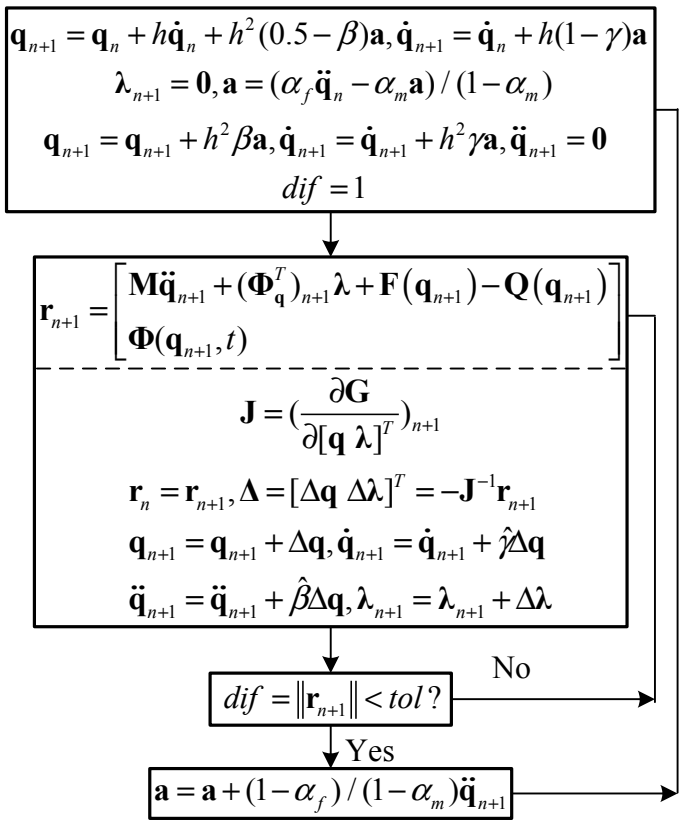

Fig. 6. The numerical iteration procedure for the generalized-α method.

As observed from the flowchart of Fig. 6, it is not necessary to evaluate the Jacobian matrix and the partial derivation term in each iteration because of the introduction of the Broyden-Newton iteration. In addition, the most cumbersome task is the evaluation of the tangent matrix of the elastic force. Therefore, with the intent to improve computation efficiency in simulation, the invariant matrix method [63] can be employed.

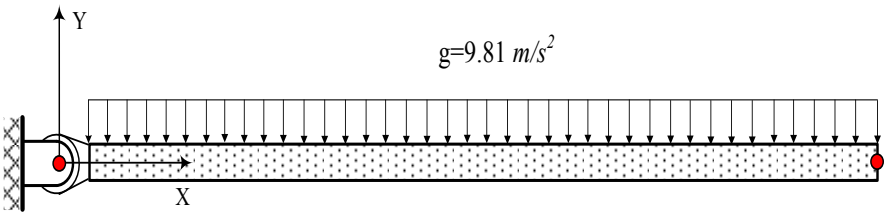

Fig. 7. Initial configuration of single pendulum.

It is important to mention that there are other alternative and robust methods to deal with the nonlinear dynamic problem, especially when large deformations and long time simulations are considered, as it has been proposed by Bathe [64]. In fact, for long time simulations the generalized-α method with large step can lead to some numerical problems, such as the divergence of the system's solution. In order to better understand the main implications of the issue a simple pendulum is considered as an application example to compare the generalized-α and the Bathe methods. Figure 7 shows the initial configuration of the simple pendulum which is acted by a uniform distributed gravitational force [65]. The length of the pendulum is 1 *m* and the cross section is a square with 0.02 *m* each side width. The Young's elasticity modulus and Poisson's ratio are 6e7*Pa* and 0.3, respectively. The material density is equal to 6000Kg/m^3. Furthermore, the arm pendulum is discretized by 5 ANCF-based elements. A long time simulation equal to 20s was performed for both methods. In addition, 4 different time steps and 4 different values of the σ-parameter of the generalized-α method were considered in the analysis, being the admissible integration error equal to $1e^{-6}$. The simulations were performed on a PC with an Intel Pentium 1.5 GHz processor and 1GB RAM. Table 2 shows the total CPU time in seconds. The outcomes of the numerical simulations are listed in Tab. 1, from which it can be

observed how important is the choice of the method utilized, as well as the selection of the σ-parameter in the case of the generalized-α method, mainly for long time simulations and large time steps. In general, the generalized-α method is more efficient from computational point of view, because the Newton iterative approach has to be carried out twice in the Bathe's scheme. Nevertheless, the Bathe's scheme is more robust, stable and quite interesting for long time simulations since larger time steps can be used. The interested reader in the details of Bathe's scheme is referred to references [64, 66, 67]. However, when a multibody system includes joints with clearance, small time steps have to be used, and special attention should be paid to detect the precise instant of contact [68]. Take, for instance, a system in which before the first impact, not only the bodies move slowly relative to each other but also the complete system is moving with an almost constant velocity. In this phase, the step size of the integration algorithm may become relatively large, being the global motion of the system characterized by relatively large translational and rotational displacements during a single time step. Therefore, if the numerical integration is not handled properly, the first impact between the colliding bodies may be observed with a high penetration depth, and, consequently, the calculated contact forces becomes artificially large. Then, smaller time steps must be considered, which increases the computation time, and, therefore, the generalized-α method is more efficient for these cases. Furthermore, the influence of the value of the algorithm σ-parameter on the outcomes is not significant since for small integration time steps this effect can be neglected.

Tab 1: Total computation time for the Bathe and generalized-α methods expressed in seconds.

Integration time step		0.001	0.004	0.01	0.05
Bathe scheme		3995.8	1029.5	667.3	248.2
Generalized-α	σ=1.0	2004.8	527.37	Not converge	
	σ=0.8	2058.1	512.5	349.8	Not converge
	σ=0.5	2042.5	518.9	376.9	152.19

	σ=0.2	2055.2	517.1	391.5	187.17

6. Results and discussion

6.1. Spatial double pendulum

In order to examine the effectiveness of the formulation presented in this work, a double pendulum with the initial configuration shown in Fig. 8 is studied here. The double pendulum is made up of three bodies, the ground body and two arms. The two arms are modeled as flexible bodies. One perfect spherical joint connects the first arm to the ground, while a spherical joint clearance exists between the two arms, resulting in a spatial multibody system with nine rigid body degrees of freedom. The system is released from the initial position with null velocities and under the action of gravity acting in the negative *Y* direction. Thus, the heights of centers of mass of all bodies dominate the total potential system energy and control the dynamic behavior of the system. The gravitational acceleration of 9.81 m/s^2 is used in the study. The link lengths are *OA*=0.3 *m* and *AB*=0.3 *m*. The cross section of the spatial beam element is a square with 0.01 *m* each side width. The material Poisson's Ratio is 0.3 and the coefficient of restitution of the contacting bodies is equal to 0.9. The spherical joint with clearance is characterized by a socket and ball radii equal to 0.02 and 0.018 *m*, respectively. For the case of lubricated spherical joint, the dynamic lubricant viscosity is chosen as 400 *cP*. The restitution coefficient c_e is set as 0.9 and the specified nonlinear index *n* is set as 1.5.

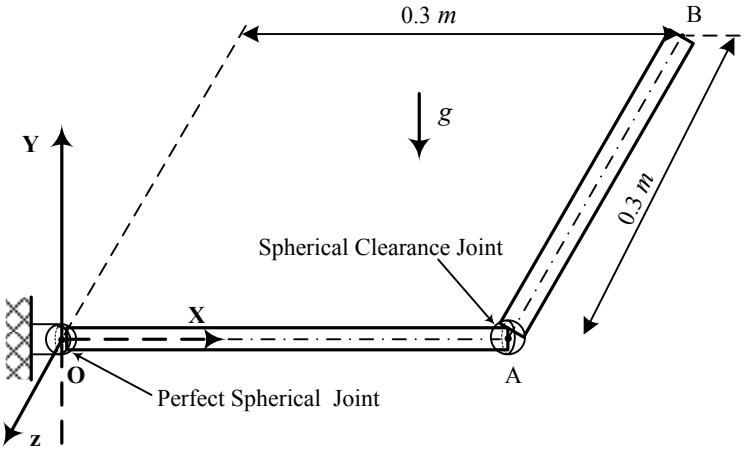

Fig. 8. Spatial double pendulum modeled by two flexible bodies and two spherical joints.

A total simulation time equal to 2 *s* is considered. The simulations are carried out by using different models and with different elements and, consequently, different values of the material Young's modulus. For the material Young's modulus E=2.07e11Pa, the material density ρ is set as 7800Kg/m^3, while for E=6e7Pa, ρ=6000 Kg/m^3. The system with E=2.07e11Pa is named here as stiff system, since its behavior is similar to that of a rigid body. In order to study the influence of the spherical joint model (dry and lubricated formulations) on the global performance of the double pendulum, kinematic and dynamic characteristics are presented and discussed in what follows. The results are compared to those obtained with a simulation in which all joints are considered to be ideal or perfect. Finally, with the intent to validate this approach, the same double pendulum is simulated using the commercial MSC.ADAMS software, and the global results are analyzed and discussed.

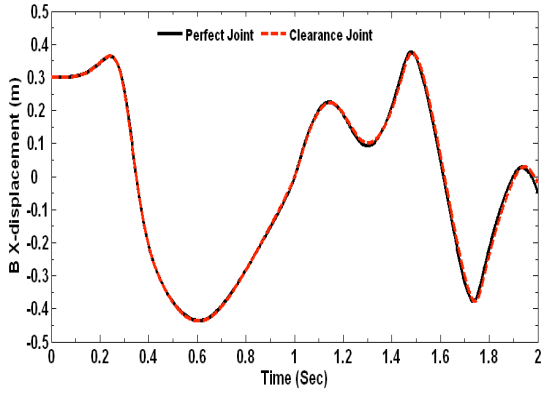

(a) 6 elements and E=2.07e11 Pa.

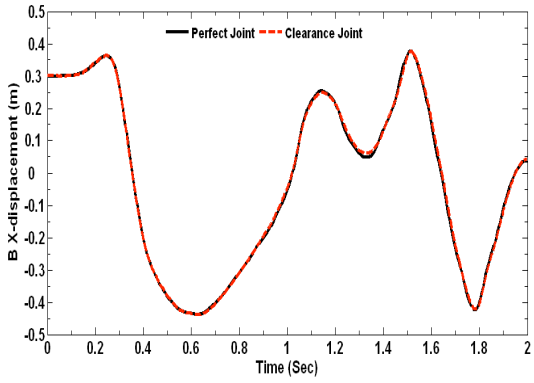

(b) 6 elements and E=6e7 Pa.

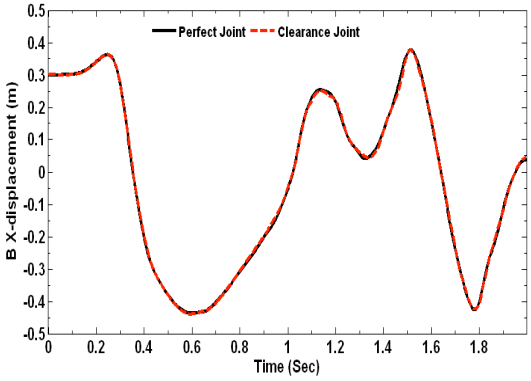

(c) 10 elements and E=6e7 Pa.

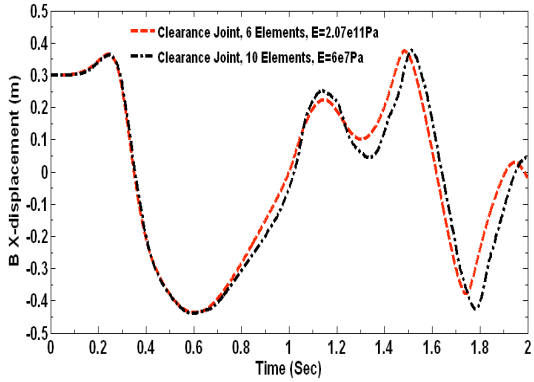

(d) E=2.07e11 Pa and E=6e7 Pa.

Fig. 9. Influence of the joint model, number of elements used in the flexible body

discretization and material Young's modulus on the *X* displacement of point *B*.

Figure 9 shows the displacement in *X* direction of point *B* for different joint models, for different number of elements used in the flexible body discretization and for two different values of Young's modulus. By observing the results plotted in Figs. 9a and 9b, it can be concluded that the system's response is not affected by the joint model, being the displacement of point *B* equal for the case of perfect joint and for the case of joint clearance. Another conclusion is that the number of elements used does not influence the displacement of point *B*, as Figs. 9b and 9c shown. However, when the system is modeled with the Young's modulus equal to *E*=6e7*Pa*, its amplitude response is larger than for the case of *E*=2.07e11*Pa*. These differences are clearly visible in the plots of Fig. 9d. It should mentioned that the system's behavior for the case of *E*=2.07e11*Pa* is similar to that when the system is modeled with rigid bodies.

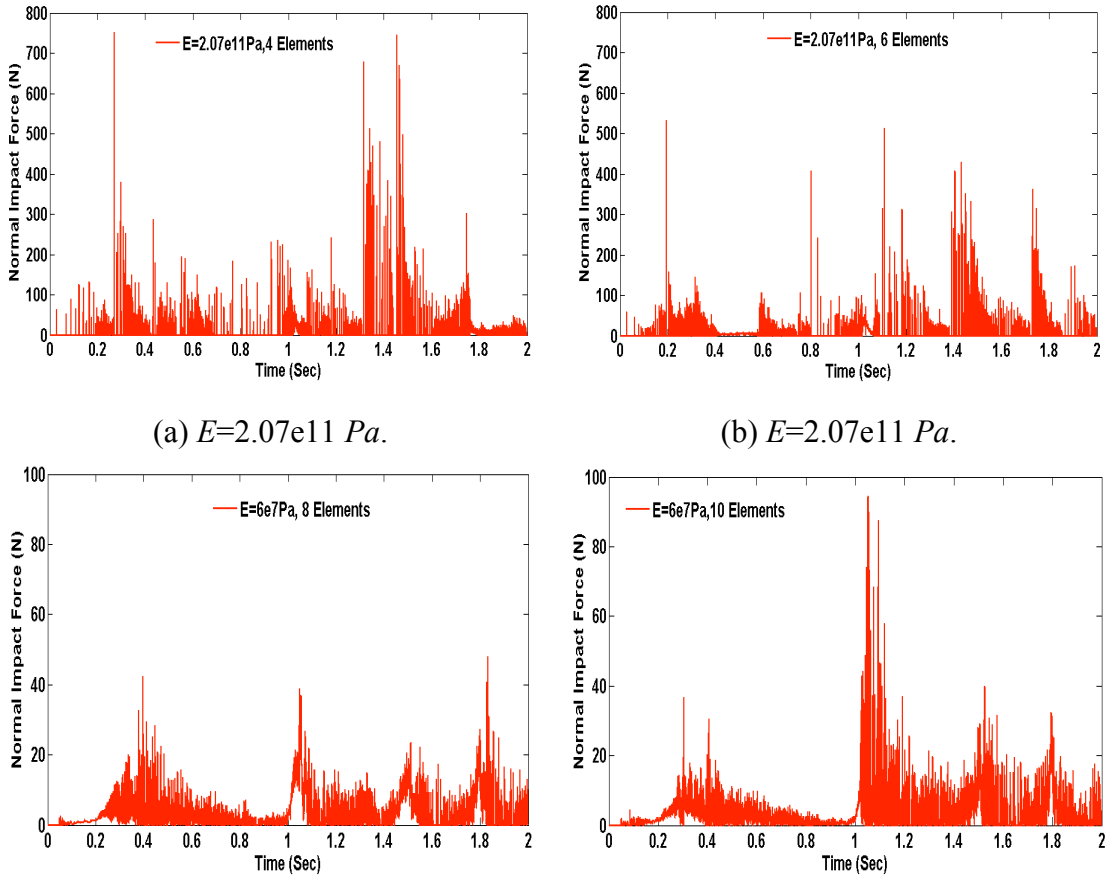

(a) *E*=2.07e11 *Pa*. (b) *E*=2.07e11 *Pa*.

(c) *E*=6e7 *Pa*. (d) *E*=6e7 *Pa*.

Fig. 10. Influence of the number of elements used in the flexible body discretization on the normal contact force.

The influence of the number of elements used in the flexible body discretization on the normal contact force can be observed in the plots of Fig. 10, which represent the evolution of the contact force with time and for two different values of the Young's modulus. By analyzing the results of Fig. 10, it can be concluded that the higher number of elements produces contact forces with lower magnitudes. This observation can be explained as with fewer elements (more system flexibility), the relative deformations are greater. Consequently, the contact forces are also greater, as the force is a function that directly depends on the deformations. The same conclusion can be drawn from the plots of Fig. 11, where the contact force versus penetration is plotted for the first impact. In this figure, it is also possible to observe the energy dissipation during the impact process as the area inside the hysteresis contact force-deformation region.

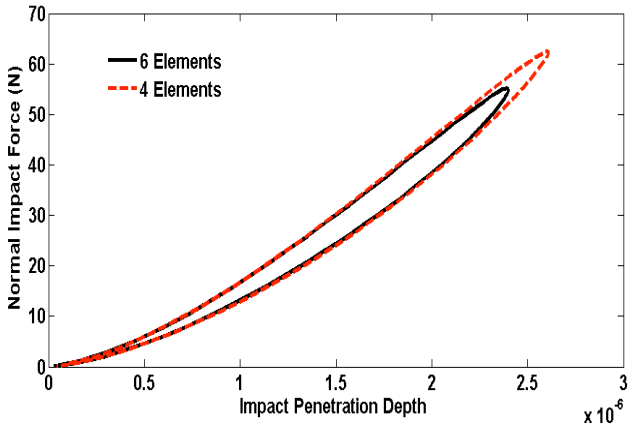

Fig. 11. Normal impact force evolution for the first impact (E=2.07e11Pa).

Figure 12 presents the plots of the transverse displacement of point B for different number of elements used in the flexible body discretization and for different joint models. It can be observed that for the point B, transverse displacements for the system with joint clearance are larger than for system with perfect joint. Furthermore, the transverse displacements for the flexible system are much larger than the transverse displacements for the stiff system. In addition, the effect of the Young's modulus is also visible in the outcomes plotted in Fig. 12.

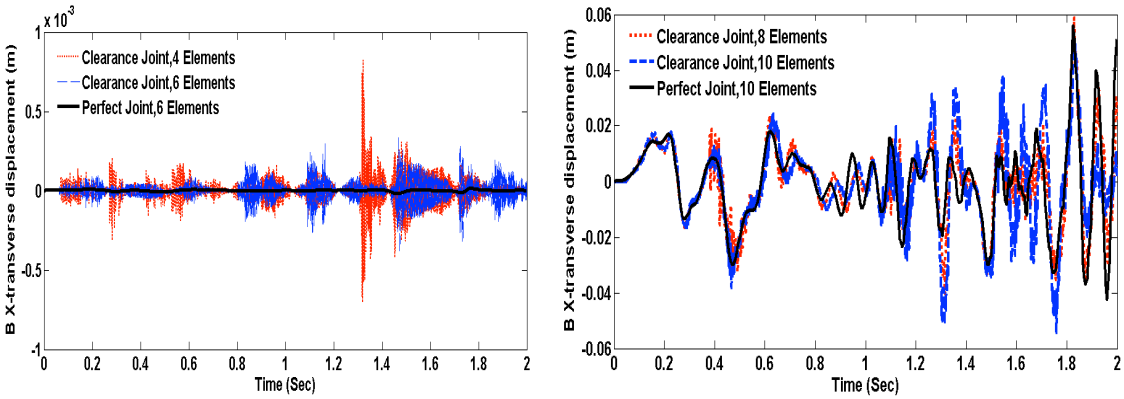

(a) E=2.07e11 Pa. (b) E=6e7 Pa.

Fig.12. Transverse displacement of point B for different number of elements used in the flexible body discretization and for different joint models.

For the case of spherical joint clearance model, the ball center trajectories relative to the socket center are illustrated in Fig. 13. With the intent to keep the figures clear and readable, only data relative to the first 0.03s of simulation are plotted. It should be noted that radius of the ball shown in Figs. 13a and 13b is equal to the clearance size used this example. By analyzing Fig. 13, it can be concluded that the penetration depth for the flexible system is larger than the penetration depth for the stiff system. It is also possible to observe the different modes of motion between the ball and socket, namely, the free flight motion, impact with rebound, and continuous contact. In the free flight motion, the ball moves freely inside the socket boundaries, that is, the ball and the socket are not in contact, hence, there is no joint reaction force. In the impact mode, which occurs at the termination of the free flight motion, impact forces are applied to the system. This mode is characterized by an abrupt discontinuity in the kinematic and dynamic responses, and a significant exchange of momentum occurs between the two impacting bodies. At the termination of the impact mode, the ball can enter either in free flight or in the following mode. In the continuous contact or following mode, the ball and the socket are in permanent contact and a rolling or sliding motion relative to each other exists. This mode ends when the ball and socket separate from each other and the ball enters in free flight mode [12].

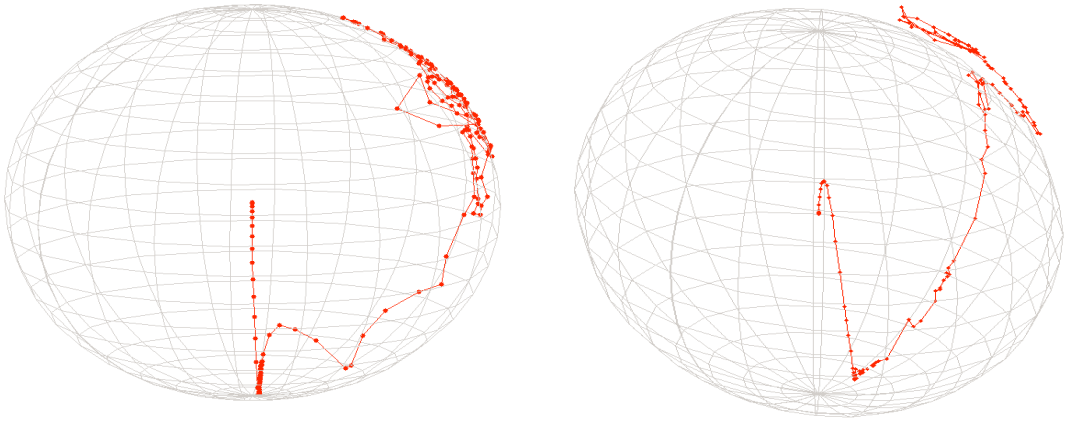

(a) 6 elements and *E*=2.07e11 *Pa*. (b) 10 elements and *E*=6e7 *Pa*.

Fig. 13. Ball center trajectories for the spherical clearance joint model.

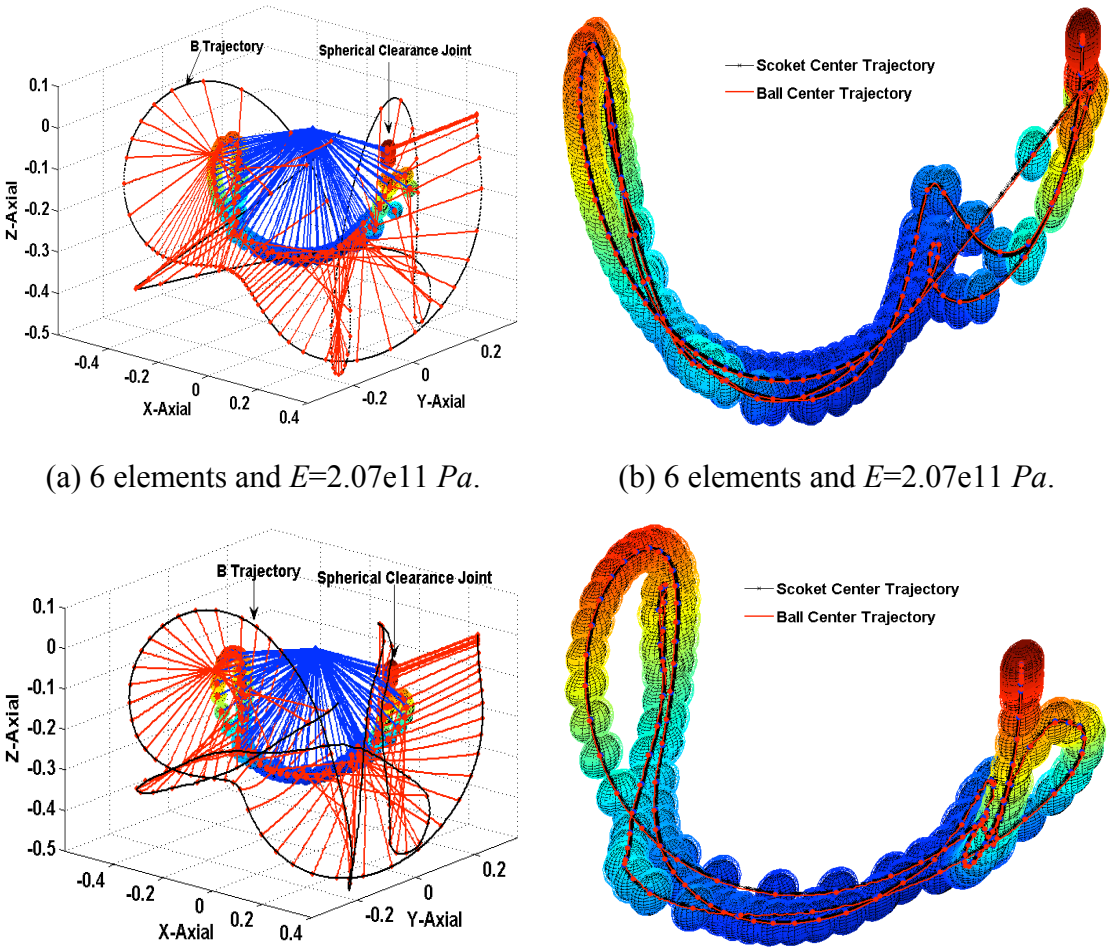

(a) 6 elements and *E*=2.07e11 *Pa*. (b) 6 elements and *E*=2.07e11 *Pa*.

(c) 10 elements and *E*=6e7 *Pa*. (d) 10 elements and *E*=6e7 *Pa*.

Fig. 14. Animation sequence of the double pendulum for stiff and flexible cases.

Figure 14 shows the global trajectory described by point *B* for the spherical clearance model and considering the stiff and flexible situations. From Figs. 14a and 14c, it can be observed that trajectory of point *B* is smoother for the stiff case compared with the one for the flexible case. The sequence simulation is enlarged in Figs. 14b and 14d, from which the detail impact process between the socket and the ball surfaces can be observed.

The above results were obtained using the spherical clearance model without taking into account the lubrication effect. Thus, in what follows, the spherical lubrication model presented in section 4 and summarized in Eq. (35), is considered in the dynamic simulation of the double pendulum. In Fig. 15 the main differences in the displacement and velocity in *X* direction of point *B* for dry and lubricated models is presented. Since the value of clearance is low, the differences at the displacements level are not significant. However, the velocities for the dry clearance case present some peaks associated with the contacts that occur between the ball and socket surfaces. Obviously, for the lubricated model, the velocities are smoother and closer to the perfect joint response due to the damping effect of the lubricant. The same conclusions can be drawn from Fig. 16 in which the transverse displacement of point *B* is plotted. In fact, the dry impact force produces larger transverse displacements than those obtained with perfect kinematic joints.

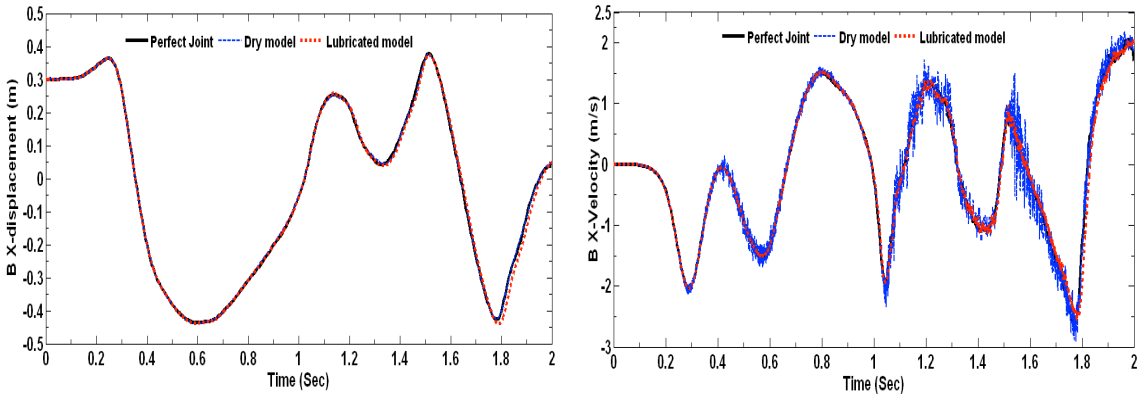

(a) Displacement. (b) Velocity.

Fig. 15. Displacement and velocity in the *X* direction of the point *B* (*E*=6e7*Pa*).

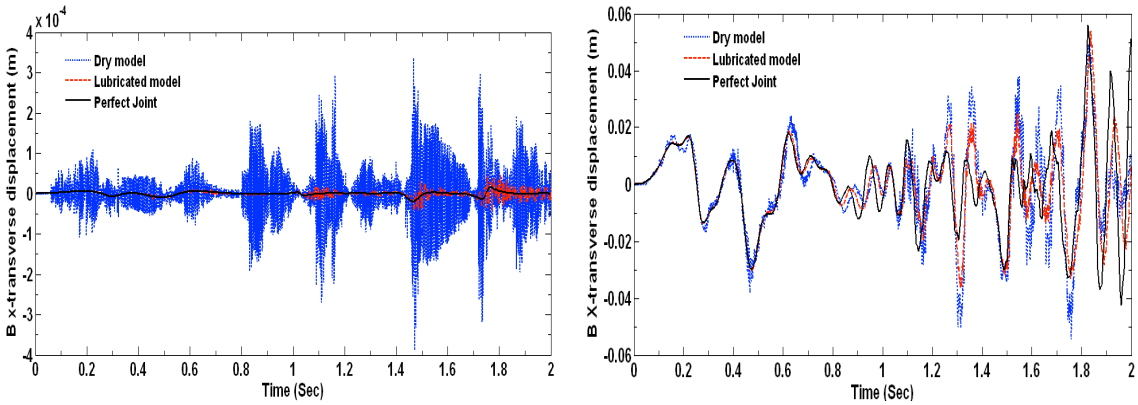

(a) 6 elements and *E*=2.07e11 *Pa*. (b) 10 elements and *E*=6e7 *Pa*

Fig. 16. Transverse displacement of point *B* for different joint models.

Figure 17 shows the plots for the eccentricity variable when dry and lubricated spherical joint models are utilized. It can be observed that, for the case of lubrication model, the magnitude of eccentricity is smaller than for the dry situation. This is due to the fact that in the lubrication model, there is no direct contact-impact between the ball and socket walls because of the presence of the lubricant. The same phenomenon can be observed in Fig. 18, which presents the ball center trajectories inside the socket boundaries. Again, with the intent to keep the figures clear and readable, only data relative to the first 1.0s of simulation are plotted. It should be highlighted that this phenomenon associated with the presence of the lubricant is a benefit from the mechanical system performance point of view and parts life.

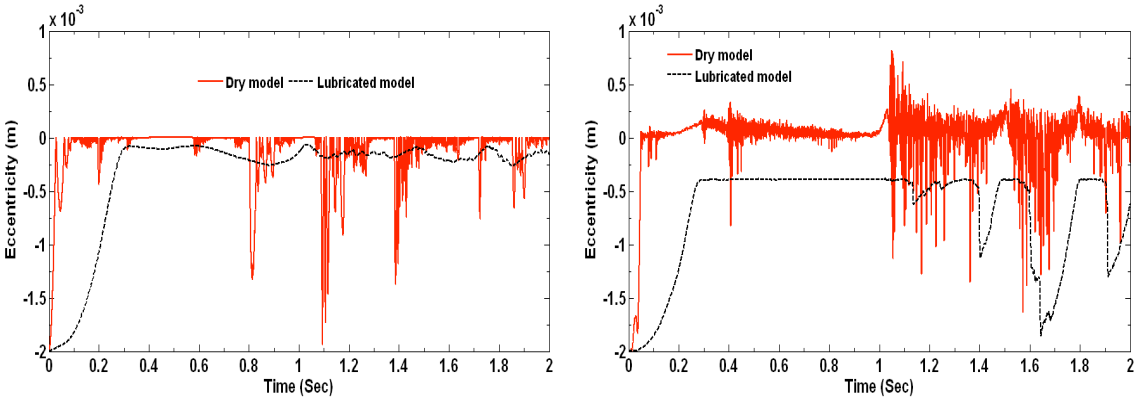

(a) 6 elements and *E*=2.07e11 *Pa*. (b) 10 elements and *E*=6e7 *Pa*

Fig. 17. Eccentricity for different spherical clearance joint models.

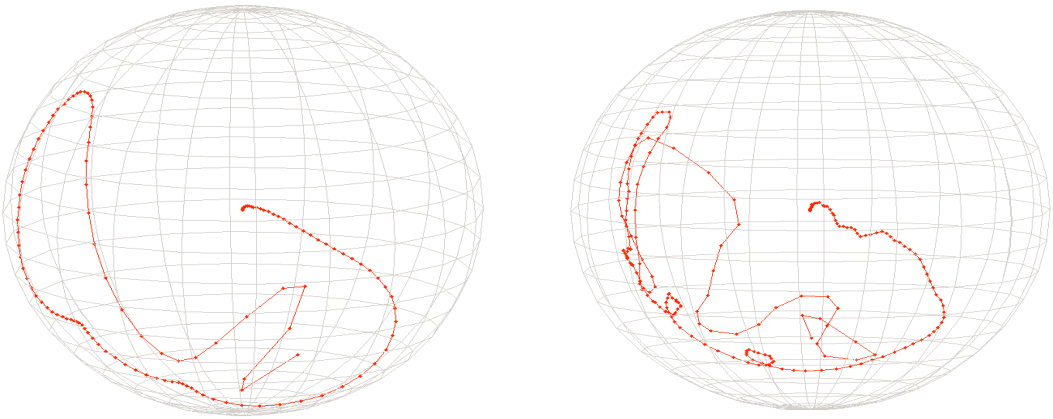

(a) 6 elements and E=2.07e11 Pa. (b) 10 elements and E=6e7 Pa

Fig. 18. Ball center trajectories for the spherical lubricated joint model.

Finally, in order to validate the approach presented in this paper, the same double pendulum was simulated using the MSC.ADAMS software for the stiff case (E=2.07e11 Pa). The option to simulate the stiff case only is due to the fact that this software is a multi-rigid-body package. Figure 19 shows the ADAMS model of the double pendulum system, in which the spherical joint clearance is modeled by a two massless spheres and corresponding constraints and contact-impact condition are set. One of the balls has 0.02 m of radius and is connected to the arm OA, the other ball with a radius 0.018 m is linked to arm AB, such that the two balls together compose a spherical joint clearance. In order to keep the analysis simple and short, only the results for the displacement of point B in the X direction are plotted, as it is illustrated in Fig. 20. The observed correlation validates the methodology presented in this study.

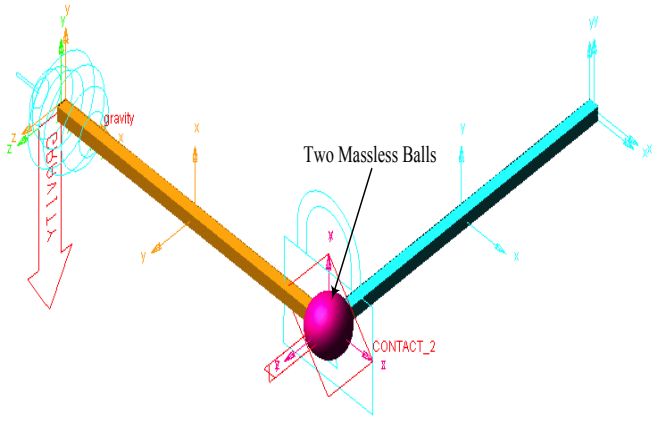

Fig. 19. MSC.ADAMS double pendulum model with a spherical joint clearance.

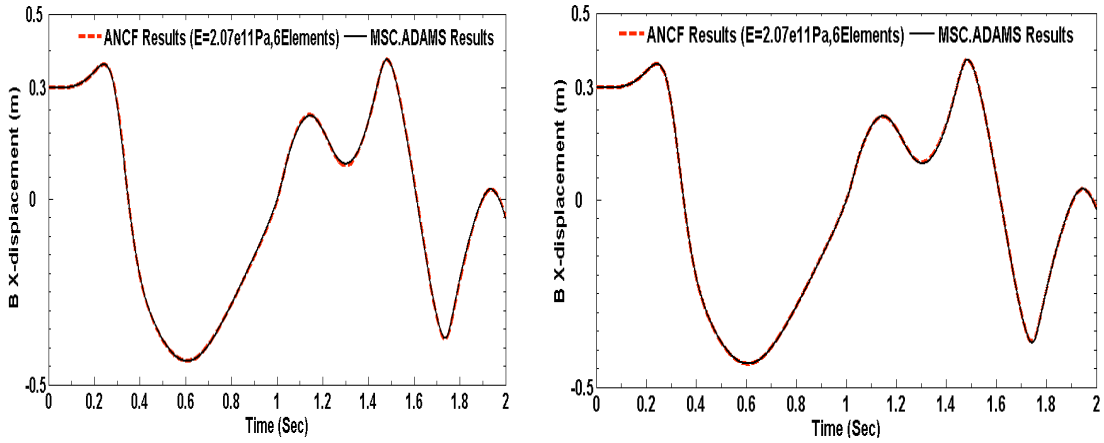

(a) Model with perfect joint. (b) Model with joint clearance.

Fig. 20. Displacement of point *B* in the *X* direction for different joint models.

6.2. Spatial four-bar mechanism

In this section, a spatial four bar mechanism is used as an illustrative example to demonstrate how the spherical joint clearance models affect the behavior of the mechanism. Figure 21 represents the initial configuration of the four bar mechanism and includes the main geometric definitions. The kinematic joints of this multibody system include two ideal three-dimensional revolute joints, connecting the ground to the links *OA* and *BH*, and one perfect spherical joint that connects the links *AB* and *BH*. A spherical joint, with a given clearance, interconnects the links *OA* and *AB*. Therefore, this four bar mechanism has a total of five rigid body degrees of freedom. The system is driven by a variable torque applied to the crank arm *OA*.

The spherical joint modeled with clearance is characterized by the socket and ball radii equal to 0.030 and 0.029 *m*, respectively. The material Poisson's ratio is set to 0.3 and the coefficient of restitution of the contacting bodies is equal to 0.9. The specified nonlinear index *n* is set as 1.5. For the case of lubricated spherical joint, the dynamic lubricant viscosity is chosen as 400 *cP*. The mechanism consists of four bodies, being three of them modeled as rigid. The links *OA* and *BH* are considered rigid with their mass centers located at mid points *G* and *F*, respectively. The inertia properties of each rigid link body are set as $I_{\eta 1}=I_{\eta 2}=3.12\times10^{-5}$ $Kg\cdot m^2$ and $I_{\zeta 1}=I_{\zeta 2}=I_{\xi 1}=I_{\xi 2}=8.93\times10^{-4}$ $Kg\cdot m^2$. The link *AB* is modeled as a flexible body discretized by five elements, and the cross section of the spatial beam element is squared shape

with 0.02 *m* side width.

In order to study the influence of the spherical clearance model in the global behavior of the spatial four bar mechanism, some kinematic and dynamic characteristics, corresponding to the first four seconds of the simulation, are presented and discussed in what follows. The results are compared to those obtained with a simulation in which all kinematic joints are considered to be ideal or perfect. The simulations are carried out by using different joint models and with different material properties. For the material Young's modulus E=2.07e11Pa, the material density ρ is set as 7800Kg/m^3, while for E=6e7Pa, ρ=6500 Kg/m^3. As in the previous example, here the system with E=2.07e11Pa is named as stiff system.

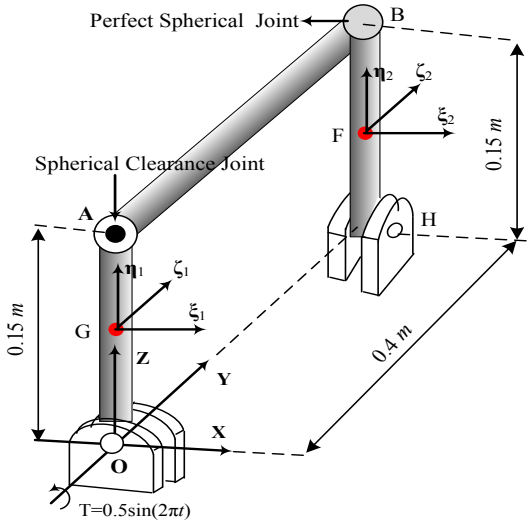

Fig. 21. Spatial four-bar mechanism which includes a spherical joint clearance.

Figure 22 presents the evolution of displacement and velocity of point B in the Y direction obtained in the simulations. These results are for different joint models and for the stiff case. In general, there are no significant differences in the displacement curves, as it can be observed in Fig. 22a. In sharp contrast, the velocity profiles indicate visible differences, namely in regard to the joint clearance model. Due to the impact between the ball and socket the velocity presents jumps clearly associated with those impacts. However, when the joint is modeled as a lubricated joint, the results are comparable to those obtained with a perfect kinematic joint. This is due to the fact that the lubricant acts as a dissipater or damper, avoiding the direct contact-impact between the ball and socket surfaces.

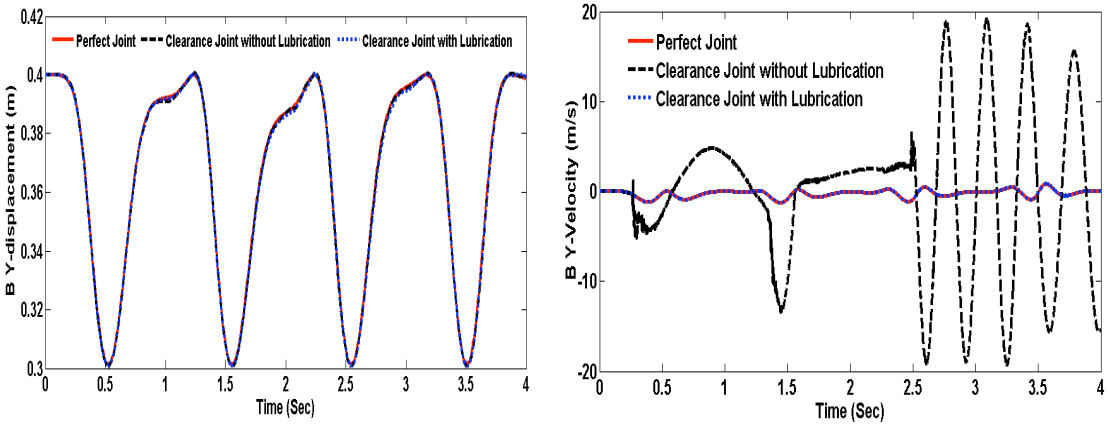

(a) Displacement. (b) Velocity.

Fig. 22. Displacement and velocity in the *Y* direction of the point *B* (*E*=2.07e11*Pa*).

The evolution of the contact and lubrication forces over the simulations is presented in the diagrams of Fig. 23, from which the precise instants where the large and sudden peak forces occur can be observed. Furthermore, it can be drawn that for the dry contact situation the magnitude of the joint reaction forces are greater than for the lubricated case, as it would be expected.

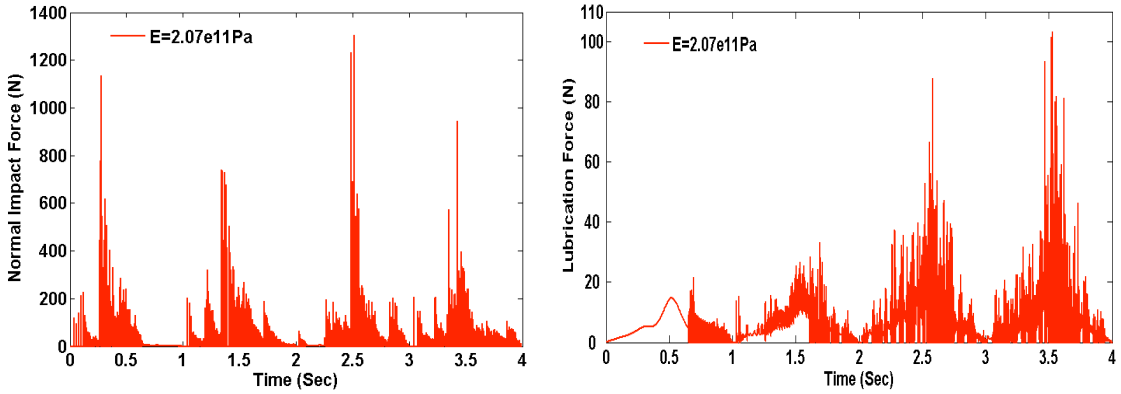

(a) Dry model. (b) Lubricated model.

Fig. 23. Joint reaction forces produced at the spherical joint clearance.

Figure 24 shows the influence of the joint model on the displacement and velocity of the point *B* in the *Y* direction for the flexible system case. As it can be seen, the joint model clearly influences the system response, mainly for the dry joint clearance model. In a similar way to the stiff case, the system performance with lubricated joint is closer to that of the perfect joint.

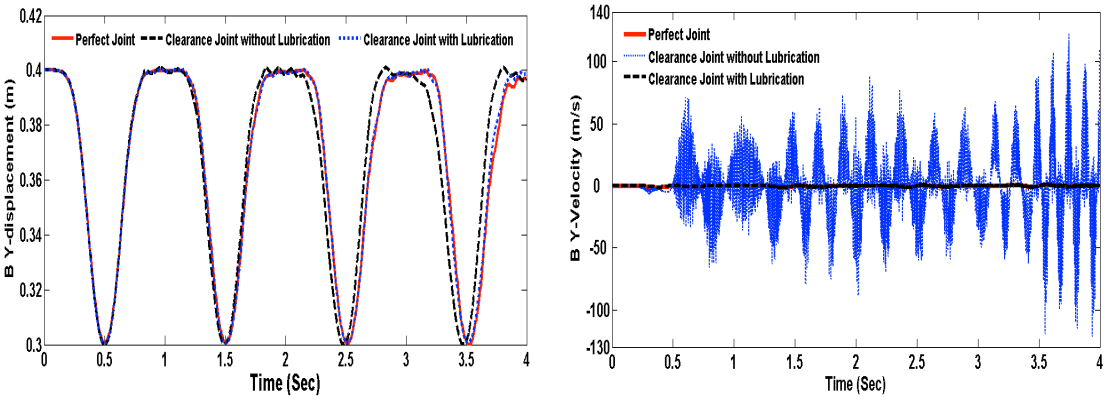

(a) Displacement. (b) Velocity.

Fig. 24. Displacement and velocity in the *Y* direction of the point *B* (*E*=6e7*Pa*).

Figure 25 shows the plots for the eccentricity variable when a dry clearance and lubricated spherical model are used. It can be observed that the eccentricities for the lubricated model are smaller than those obtained by dry contact model. The effect of Young's modulus is also visible in Fig. 25. The same phenomenon can be seen in Figs. 26 and 27 which present the ball center trajectories inside the socket boundaries. For Fig. 26, with the intent to keep the figures clear and readable, only data relative to the first 0.3s of simulation are plotted, while for Fig.27 only data relative to the first 1s of simulation are plotted. In order to keep the figures clear and readable, only data relative to the first instants of simulation are plotted. For the lubricated joint model, the ball center moves closer to its center than for the dry contact model due to the presence of the lubricant.

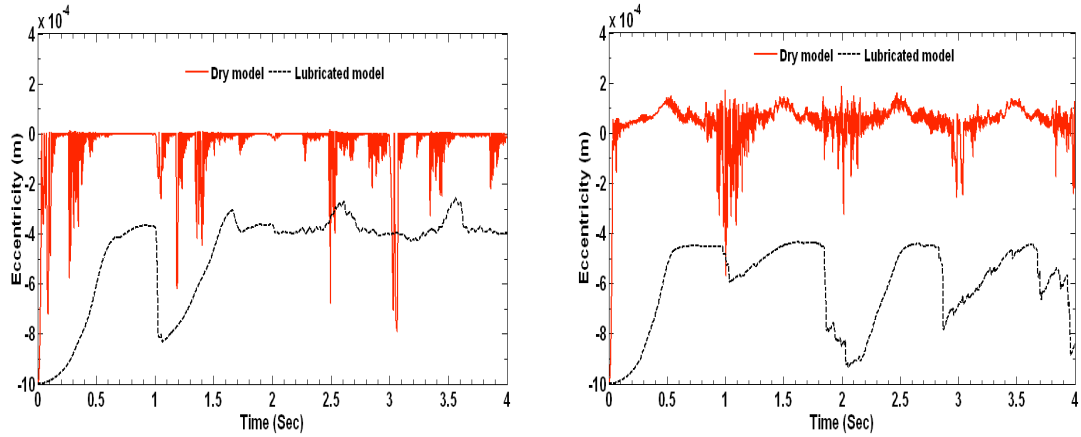

(a) *E*=2.07e11 *Pa*. (b) *E*=6e7 *Pa*

Fig. 25. Eccentricity for difference spherical clearance joint models.

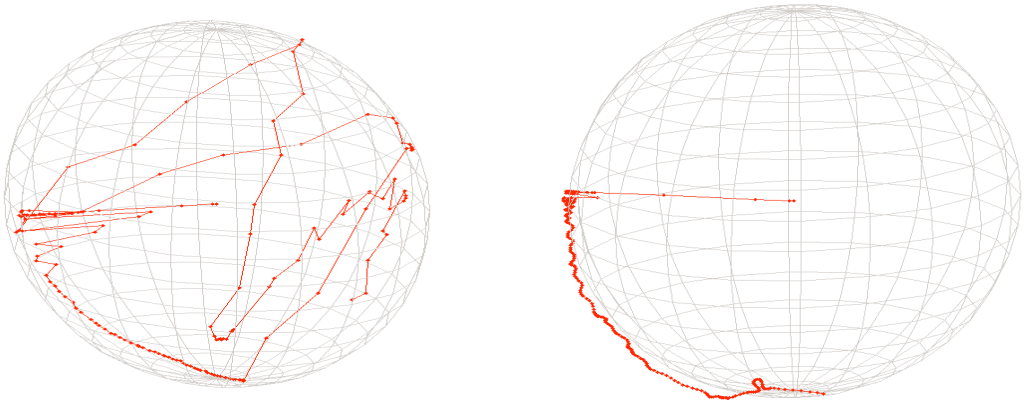

(a) E=2.07e11 Pa. (b) E=6e7 Pa

Fig. 26. Ball center trajectories for the spherical joint clearance model.

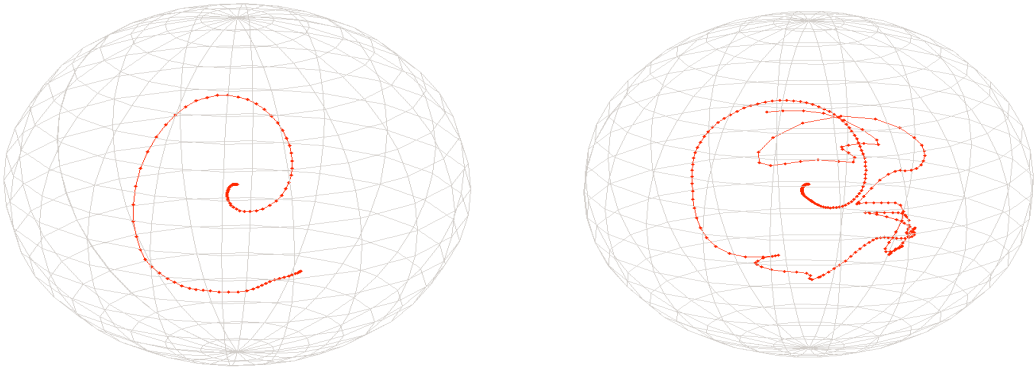

(a) E=2.07e11 Pa. (b) E=6e7 Pa

Fig. 27. Ball center trajectories for the spherical lubricated joint model.

Finally, in a similar way to the previous example, the spatial four bar mechanism was simulated in the commercial MSC.ADAMS software for different situations. Similar to the first example, Figure 28 shows the ADAMS model of the spatial four bar mechanism, in which the spherical joint clearance is modeled by a two massless balls and corresponding constraints and contact-impact condition are set. In order to keep the analysis simple and short, only the outcomes for displacement of point B in the Y direction are plotted, as it is illustrated in Fig. 29. The correlation observed allows to validate the methodology presented in the present work.

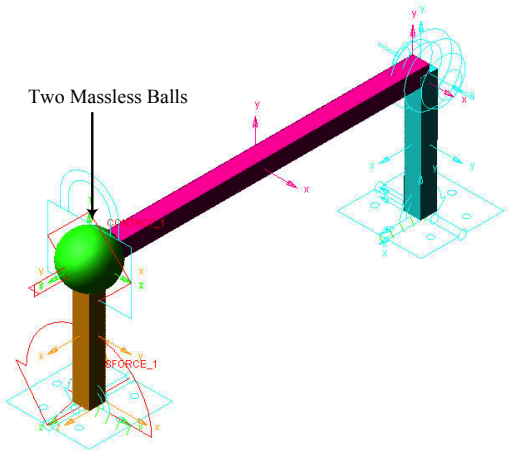

Fig. 28. MSC.ADAMS four bar mechanism model with a spherical joint clearance.

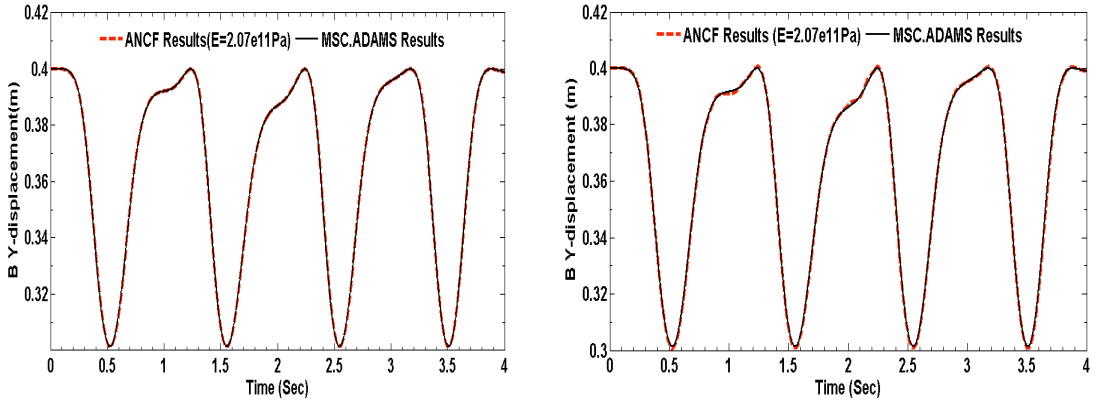

(a) Model with perfect joint. (b) Model with joint clearance.

Fig. 29. Displacement of point *B* in the *X* direction for different model.

7. Conclusions

In this paper, a general and comprehensive methodology for the dynamic modeling and analysis of spatial flexible systems with clearances and lubricated joints has been presented. The absolute nodal coordinate method is used to formulate the dynamics of flexible multibody systems. The equations of motion incorporate the contact-impact forces due to the collisions of the bodies that constitute the joint clearances, as well as the lubrication forces produced when the fluid lubricant action is considered. In the joint model with clearance, the intra-joint contact forces are evaluated according to a modified Hertzian-based contact law, which includes a damping term to account for the energy dissipation. The friction phenomenon is

included through a modified Coulomb's friction law. In the case of lubricated joints, the resulting lubrication forces are derived by employing the corresponding Reynolds' equation. Furthermore, suitable models for spherical joint clearances for dry and lubricated cases are embedded into the multibody systems equations of motion. The generalized-**α** method is used to solve the system equations of motion with constant system mass matrix based on the absolute nodal coordinate method. To improve computation efficiency, the invariant matrix method is used.

The effectiveness of the approach presented here is demonstrated throughout the dynamic simulation of two spatial multibody systems that include perfect, clearance and lubricated joints, namely, an open-loop system, the spatial double pendulum, and a closed-loop system, the spatial four bar mechanism. The influence of the flexibility of bodies and the joint models is investigated, as the main contribution of the paper, not studied literature. In general, the results evidence that the contact forces obtained by using the relative flexible system model are smaller than those obtained with rigid system model. In addition, results demonstrate that the direct ball-socket impact can be avoided when a fluid lubricant is introduced in the joint. This leads to a performance of the system with lubricated joint closer to the perfect joint case. In order to verify and validate the methodology presented in this paper, some results are compared to those obtained by using the MSC.ADAMS software, but only for the stiff system case. The simulation results indicate that the methodology for modeling and dynamics analysis of spatial flexible multibody systems with spherical joint clearance and lubrication condition based on the absolute nodal coordinate method is valid and effective.

Acknowledgments

We would like to thank Prof. Daniel García-Vallejo from University of Seville, Spain, and Dr. Johannes Gerstmayr from Johannes Kepler University of Linz, Austria, for their great help with the ANCF method. Finally, we would also like to acknowledge the anonymous reviewers for their insightful comments and suggestions on an earlier draft of this paper.

References

[1] Flores P, Ambrósio J. Revolute joints with clearance in multibody systems. Computers and Structures 2004;82: 1359-1369.

[2] Liu C-S, Zhang K, Yang R. The FEM analysis and approximate model for cylindrical joints with clearances. Mechanism and Machine Theory 2007;42:183-197.

[3] Crowthera AR, Singha R, Zhangb N, Chapman C. Impulsive response of an automatic transmission system with multiple clearances: Formulation, simulation and experiment. Journal of Sound and Vibration 2007;306: 444-466.

[4] Bouzidane A, Thomas M. An electrorheological hydrostatic journal bearing for controlling rotor vibration. Computers and Structures 2008;86:463-472.

[5] Dubowsky A, Freudenstein F. Dynamic analysis of mechanical systems with clearances, part 1: formulation of dynamic model. Journal of Engineering for Industry 1971;93(1):305-309.

[6] Dubowsky S, Freudenstein F. Dynamic analysis of mechanical systems with clearances, part 2: Dynamics Response. Journal of Engineering for Industry 1971;93(1):310-316.

[7] Miedema B, Mansour WM. Mechanical Joints with Clearance: a Three-Mode Model. Journal of Engineering for Industry 1976;98(4):1319-1323.

[8] Turvey GJ, Wang P. An FE analysis of the stresses in pultruded GRP single-bolt tension joints and their implications for joint design. Computers and Structures 2008;86:1014–1021.

[9] Srivastava N, Haque I. Clearance and friction-induced dynamics of chain CVT drives. Multibody System Dynamics 2008;19(3):255-280.

[10] Flores P, Ambrósio J, Claro JCP, Lankarani HM, Kinematics and Dynamics of Multibody Systems with Imperfect Joints: Models and Case Studies. Berlin: Spinger; 2008.

[11] Liu C-S, Zhang K, Yang L. Normal force-displacement relationship of spherical joints with clearances. Journal of Computational and Nonlinear Dynamics 2006;1(2):160-167.

[12] Flores P, Ambrósio J, Claro JCP, Lankarani HM. Dynamics of multibody systems with spherical clearance joints. Journal of Computational and Nonlinear Dynamics 2006;1(3):240-247.

[13] Flores P, Ambrósio J, Claro JCP, Lankarani HM, Koshy CS. Lubricated revolute joints in rigid multibody systems. Nonlinear Dynamics 2009 (Available online 8 August 2008) doi: 10.1007/s11071-008-9399-2.

[14] Erkaya S. Uzmay I. A neural-genetic (NN–GA) approach for optimising mechanisms having joints with clearance. Multibody System Dynamics 2008;20(1):69-83.

[15] Erkaya S. Uzmay I. Determining link parameters using genetic algorithm in mechanisms with joint clearance. Mechanism and Machine Theory 2009;44(1): 222-234.

[16] Bing S, Ye J. Dynamic analysis of the reheat-stop-valve mechanism with revolute clearance joint in consideration of thermal effect. Mechanism and Machine Theory 2008;43(12):1625–1638.

[17] Flores, P. Modeling and simulation of wear in revolute clearance joints in multibody systems. Mechanism and Machine Theory 2009 (Available online 21 September 2008) doi:10.1016/j.mechmachtheory.2008.08.003.

[18] Miedema B, Mansour WM. Mechanical joints with clearance: a three-mode model. Journal of Engineering for Industry 1976;98(4):1319-1323.

[19] Hunt KH, Crossley FR. Coefficient of restitution interpreted as damping in vibroimpact. Journal of Applied Mechanics 1975;7:440-445.

[20] Lankarani HM, Nikravesh PE. A contact force model with hysteresis damping for impact analysis of multibody systems. Journal of Mechanical Design 1990;112:369-376.

[21] Pombo JC, Ambrósio JAC. Application of a wheel–rail contact model to railway dynamics in small radius curved tracks. Multibody System Dynamics 2008;19:91-114.

[22] Dubowsky S, Gardner TN. Design and analysis of multilink flexible mechanisms with multiple clearance connections. Journal of Engineering for Industry 1977;99:88-96.

[23] Dubowsky S, Deck JF, Costello H. The dynamic modeling of flexible spatial machine systems with clearance connections. Journal of Mechanisms, Transmissions and Automation in Design 1987;109:87-94.

[24] Dubowsky S, Moening MF. An Experimental and Analytical Study of Impact Forces in Elastic Mechanical Systems with Clearances. Mechanism and Machine Theory 1978;13:451-465.

[25] Kakizaki T, Deck JF, Dubowsky S. Modeling the Spatial Dynamics of Robotic Manipulators with Flexible Links and Joint Clearances. Journal of Mechanical Design 1993;115:839-84714.

[26] Bauchau OA, Bottasso CL. Contact Conditions for Cylindrical, Prismatic, and Screw Joints in Flexible Multibody Systems. Multibody System Dynamics 2001;5:251-278.

[27] Bauchau OA, Rodriguez J. Modelling of Joints with Clearance in Flexible Multibody Systems. International Journal of Solids and Structures 2002;39:41-63.

[28] Liu TS, Lin YS. Dynamic analysis of flexible linkages with lubricated joints. Journal of Sound and Vibration 1990;141(2):193-205.

[29] Shiau T-N, Tsai Y-J, Tsai M-S. Nonlinear dynamic analysis of a parallel mechanism with consideration of joint effects. Mechanism and Machine Theory 2008;43:491-505.

[30] Shabana AA. Flexible Multibody Dynamics Review of Past and Recent Developments. Multibody System Dynamics 1997;1:189-222.

[31] Shabana AA. An absolute Nodal Coordinates Formulation for the Large Rotation and Deformation Analysis of Flexible Bodies. In: Report No. MBS96-1-UIC,

University of Illinois at Chicago; 1996.

[32] Shabana AA. Definition of the Slopes and Absolute Nodal Coordinate Formulation. Multibody System Dynamics 1997;1:339-348.

[33] Shabana AA. Dynamics of Multibody Systems. 3rd ed. Cambridge New York: University Press; 2005.

[34] Eberhard P, Schiehlen W. Computational Dynamics of Multibody Systems History, Formalisms, and Applications. Journal of Computational and Nonlinear Dynamics 2006;1:3-12.

[35] Yoo WS, Dmitrochenko O, Yu D. Review of Finite Elements Using Absolute Nodal Coordinates for Large-Deformation Problems and Matching Physical Experiments. In: ASME 2005 International Design Engineering Technical Conferences and Computers and Information in Engineering Conference, California, Long Beach, DETC2005-84720.

[36] García-Vallejo D, Mikkola AM, Escalona JS. A new locking-free shear deformable finite element based on absolute nodal coordinates. Nonlinear Dynamics 2007;50:249-264.

[37] Gerstmayr J, Matikainen MK, Mikkola AM. A geometrically exact beam element based on the absolute nodal coordinate formulation. Multibody System Dynamics 2008;20(4): 359-384.

[38] Dmitrochenko O, Mikkola AM. Two simple triangular plate elements based on the absolute nodal coordinate formulation. Journal of Computational and Nonlinear Dynamics 2008;3:0410121-0410128.

[39] Shabana AA, Yakoub RY. Three-dimensional absolute nodal coordinate formulation for beam elements: theory. Journal of Mechanical Design 2001;123:606-613.

[40] Yakoub RY, Shabana AA. Three dimensional absolute nodal coordinate formulation for beam elements: implementation and applications. Journal of Mechanical Design 2001;123:614-621.

[41] Schwab AL, Meijaard JP. Comparison of three-dimensional flexible beam elements for dynamic analysis: finite element method and absolute nodal coordinate formulation. In: ASME 2005 International Design Engineering Technical Conferences and Computers and Information in Engineering Conference, California, Long Beach, DETC2005-85104.

[42] Sugiyama H, Gerstmayr J, Shabana AA. Cross-section deformation in the absolute nodal coordinate formulation. In: ASME 2005 International Design Engineering Technical Conferences and Computers and Information in Engineering Conference, California, Long Beach, DETC2005-84524.

[43] Shabana AA. Computational Continuum Mechanics. New York: Cambridge University Press; 2008.

[44] Flores P, Ambrósio J, Claro, JCP; Lankarani, HM. Influence of the contact-impact force model on the dynamic response of multi-body systems. Multibody System Dynamics 2006;220(1)21-34.

[45] Hertz H. On the contact of solids, 1881. On the contact of rigid elastic solids and

on hardness, 1882. Translated by D.E. Jones and G.A. Schott, Miscellaneous Papers, MacMillan and Co. Ltd., London (1896) 146-183.

[46] Nikravesh PE. Computer Aided Analysis of Mechanical Systems, Prentice Hall, Englewood Cliffs, New Jersey, 1988.

[47] Shivaswamy S. Modeling Contact Forces and Energy Dissipation During Impact in Multibody Mechanical Systems, Ph.D. Dissertation, Wichita State University, Wichita, USA, 1997.

[48] Shivaswamy S, Lankarani HM. Impact analysis of plates using quasi-static approach. Journal of Mechanical Design 1997;119(3):376-381.

[49] Schiehlen W, Seifried R. Three Approaches for Elastodynamic Contact in Multibody Systems. Multibody System Dynamics 2004;12(1):1-16.

[50] Flores P, Koshy CS, Lankarani HM, Ambrosio J, Claro JCP. Numerical and experimental analysis of planar multibody systems with revolute clearance joints, Proceedings of ECCOMAS Multibody Dynamics 2007, International Conference on Advances in Computational Multibody Dynamics 2007, C.L. Bottasso, P. Masarati, L. Trainelli (eds.), Milano, Italy, 25–28 June 2007, 17p.

[51] Kuwabara G, Kono K. Restitution coefficient in a collision between two spheres, Japanese Journal of Applied Physics 1987;26(8):1230–1233.

[52] Ramirez R, Poschel T, Brilliantov N, Schwager T. Coefficient of restitution of colliding viscolelastic spheres, Physical Review E 1999;60(4):4465–4472.

[53] Ahmed S, Lankarani H.M., Pereira MFOS, Frictional impact analysis in open loop multibody mechanical system. Journal of Mechanical Design 1999;121(1):119- 127.

[54] Greenwood DT. Principles of Dynamics, Prentice Hall, Englewood Cliffs, New Jersey, 1965.

[55] Ambrósio JAC. Impact of Rigid and Flexible Multibody Systems: Deformation Description and Contact Models. In: Schiehlen W, Valásek M (Eds.), Proceedings of the NATO-ASI on Virtual Non-linear Multibody Systems, Vol. II, 2002:15-33.

[56] Sopanen JT, Mikkola AM. Description of Elastic Forces in Absolute Nodal Coordinate Formulation. Nonlinear Dynamics 2003;34:53-74.

[57] Goenka PK. Effect of Surface Ellipticity on Dynamically Loaded Spherical and Cylindrical Joints and Bearings. PhD Dissertation, Cornell University, Ithaca, New York, 1980.

[58] Pinkus O, Sternlicht SA. Theory of Hydrodynamic Lubrication. New York: McGraw-Hill; 1961.

[59] Flores P, Ambrósio J, Claro JP. Dynamic Analysis for Planar Multibody Mechanical Systems with Lubricated Joints. Multibody System Dynamics 2004;12:47-74.

[60] Chung J, Hulbert G. A time integration algorithm for structural dynamics with improved numerical dissipation: The generalized-a method. Journal of Applied Mechanics 1993;60 :371-375.

[61] Arnold M, Brüls O. Convergence of the generalized-a scheme for constrained

mechanical systems. Multibody System Dynamics 2007;18(2):185-202.

[62] Broyden CG. A class of methods for solving nonlinear simultaneous equations, Mathematics of Computation 1965;19(92):577-593.

[63] García-Vallejo D, Mayo J, Escalona JL. Efficient evaluation of the elastic forces and the Jacobian in the absolute nodal coordinate formulation. Nonlinear Dynamics 2004;35:313-329.

[64] Bathe KJ. Conserving energy and momentum in nonlinear dynamics: A simple implicit time integration scheme. Computers and Structures 2007; 85: 437-445.

[65] Zhang Y, Tian Q, Chen L, Yang J. Simulation of a viscoelastic flexible multibody system using absolute nodal coordinate and fractional derivative methods. Multibody System Dynamics 2008 (Available online 28 November 2008) doi: 10.1007/s11044-008-9139-x.

[66] Bathe KJ, Baig MMI. On a composite implicit integration procedure for nonlinear dynamics. Computers and Structures 2005; 83: 2513-24.

[67] Bathe KJ. On reliable finite element methods for extreme loading conditions. Ibrahimbegovic A, Kozar I, (eds.). Extreme man-made and natural hazards in dynamics of structures. Springer Verlag, 2007:71-102.

[68] Flores, P., Ambrósio, J., On the contact detection for contact analysis in multibody systems, Proceedings XXII ICTAM, 22nd International Congress of Theoretical and Applied Mechanics, Adelaide Convention Centre, Adelaide, Australia, August 25-29, 2008, 2p.